Cell Reports

Resource

A single-cell transcriptional reference for the functional and developmental diversity of neonatal innate lymphoid cells

Graphical abstract

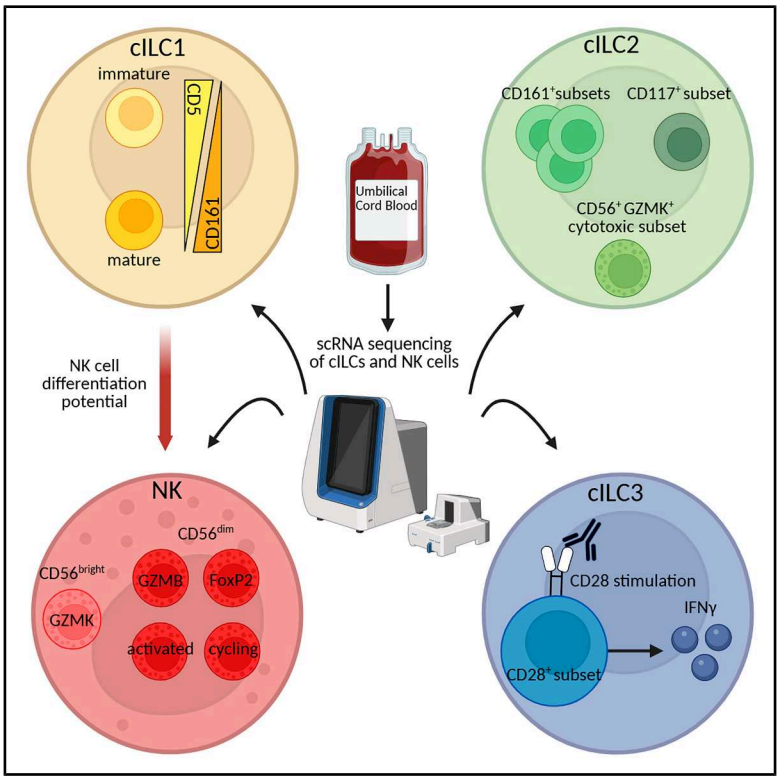

Highlights

- Unraveling the transcriptional landscape of neonatal innate lymphoid cells
- cILC1s develop into NK but not T cells in a 3D artificial thymic organoid model
- cILC2s include a putative cytotoxic subset expressing granzyme K
- cILC3s can be triggered via the CD28 pathway to produce IFNγ

Authors

Sabrina B. Bennstein, Julian Reiß, Katharina Raba, ..., Gesine Kögler, Marc D. Beyer, Markus Uhrberg

Correspondence

sabrina.bennstein1@rwth-aachen.de (S.B.B.), markus.uhrberg@med.uni-duesseldorf.de (M.U.)

In brief

This study dissects the transcriptional diversity of circulating innate lymphoid cells (cILCs) from umbilical cord blood on the single-cell level. Accompanying phenotypic, functional, and differentiation experiments establish cILC1s as restricted NK cell progenitors and identify an IFNγ-producing cILC3 subset that is responsive to stimulation via the CD28 pathway.

Bennstein et al., 2026, Cell Reports *45*, 117000
March 24, 2026
https://doi.org/10.1016/j.celrep.2026.117000

CellPress

Cell Reports

CellPress
OPEN ACCESS

Resource

A single-cell transcriptional reference for the functional and developmental diversity of neonatal innate lymphoid cells

Sabrina B. Bennstein,[1,2,6,*] Julian Reiß,[1] Katharina Raba,[1] Thi X.U. Pham,[1,3] Stefan Paulusch,[4] Elena De Domenico,[4] Tim Niehues,[3] Johannes C. Fischer,[1] Gesine Kögler,[1] Marc D. Beyer,[4,5] and Markus Uhrberg[1,*]

[1]Institute for Transplantation Diagnostics and Cell Therapeutics, Medical Faculty, Heinrich-Heine University Düsseldorf, Moorenstr. 5, 40225 Düsseldorf, Germany

[2]Institute of Immunology, Faculty of Medicine, RWTH Aachen University, 52074 Aachen, Germany

[3]Department of Pediatrics, Helios Klinikum Krefeld, Krefeld, Germany

[4]PRECISE Platform for Genomics and Epigenomics at German Center for Neurodegenerative Diseases (DZNE) and University of Bonn and West German Genome Center, Bonn, Germany

[5]Immunogenomics & Neurodegeneration, German Center for Neurodegenerative Diseases (DZNE), Bonn, Germany

[6]Lead contact

*Correspondence: sabrina.bennstein1@rwth-aachen.de (S.B.B.), markus.uhrberg@med.uni-duesseldorf.de (M.U.)

https://doi.org/10.1016/j.celrep.2026.117000

SUMMARY

Circulating innate lymphoid cells (cILCs) comprise a complex mixture of subsets with effector functions and progenitor potential toward mature ILCs and natural killer (NK) cells. Here, we dissected cord blood (CB) cILC complexity using single-cell RNA sequencing (RNA-seq) combined with developmental and functional analyses. cILC1s comprise six different subsets, with four showing different maturation degrees and two resembling NK cell progenitors. Despite previously described transcriptional similarity to T cells, the developmental potential of cILC1s was restricted to NK cells using an artificial thymic organoid (ATO) model. cILC2s could be divided into four main subsets: CD161^{+}, CD117^{+}, activated cILC2s, and cytotoxic cILC2s. Finally, a CD161^{+}CD28^{+}CD117^{low} ILC3 subset was identified that secreted IFNγ upon co-stimulation with a CD28 superagonist, suggesting an alternative activation stimulus for cILC3s. Altogether, this in-depth analysis provides a detailed picture of cILC diversity in immunologically naive CB and constitutes a versatile resource for further exploration of their translational potential.

INTRODUCTION

Human innate lymphoid cells (ILCs) are rare lymphocytes with effector functionality residing in various tissues and contributing to barrier integrity and tissue homeostasis.[1,2] In comparison to tissue-resident ILCs, circulating ILCs (cILCs) show divergent transcriptional signatures and cell surface expression patterns and do not share identical effector functionality.[3,4] Current knowledge divides cILCs into three different subsets: cILC1s, cILC2s, and cILC3s. cILC1s and cILC3s have been described to have precursor potential and effector functionality.[3,5–7] cILC2s, on the other hand, exhibit effector functionality similar to tissue-resident ILCs.[7,8] Previous studies using bulk RNA sequencing (RNA-seq) analyses showed distinct enriched gene signatures for each cILC subset, as well as properties shared between all three cILC subsets, such as the transcriptional regulator *inhibitor of DNA binding 3* (ID3).[7,9] Nevertheless, phenotypic and functional features of cILCs suggest additional transcriptional heterogeneity within cILC1s, cILC2s, and cILC3s that remains to be uncovered.[3]

cILC1s are identified as lineage-negative (Lin^{-})CD94^{-}CD127^{+}CD117^{-}CRTH2^{-} cells with moderate expression of the transcription factor (TF) T-BET.[3] In cord blood (CB), cILC1s have been previously divided into a dominant CD5^{+} cILC1 population and a less common CD161^{+} cILC1 population.[5] The latter was able to secrete IFNγ after specific interleukin stimulation.[5] Furthermore, CB and peripheral blood cILC1s showed either CD8 or CD4 expression.[5,10] In general, CD5^{+} cILC1s co-expressed more T cell-associated molecules compared to CD161^{+} cILC1s.[5] Expression of T cell-associated molecules had been previously observed on ILC1s isolated from peripheral blood and tissues.[4,11–13] Despite their different phenotypes, all four cILC1 subsets—based on CD5 and CD161 expression—were able to generate NK cells.[5] Of note, we have recently shown that a putative progenitor of cILC1s with comparable NK cell differentiation potential resides in the thymus and plays an important role in the homeostasis of cILC1s.[14]

cILC2s are identified as Lin^{-}CD94^{-}CD127^{+}CD117$^{-/+}$CRTH2^{+} cells with high expression of the TF GATA3.[7,8] cILC2s were further divided according to their CD117 expression into CD117^{high} cILC2s and CD117^{low} cILC2s.[15] CD117^{high} cILC2s co-expressed molecules typically associated with ILC3s. Depending on the stimulatory conditions, CD117^{high} cILC2s were able to secrete either IL-17A or IFNγ. CD117^{low} cILC2s, on the

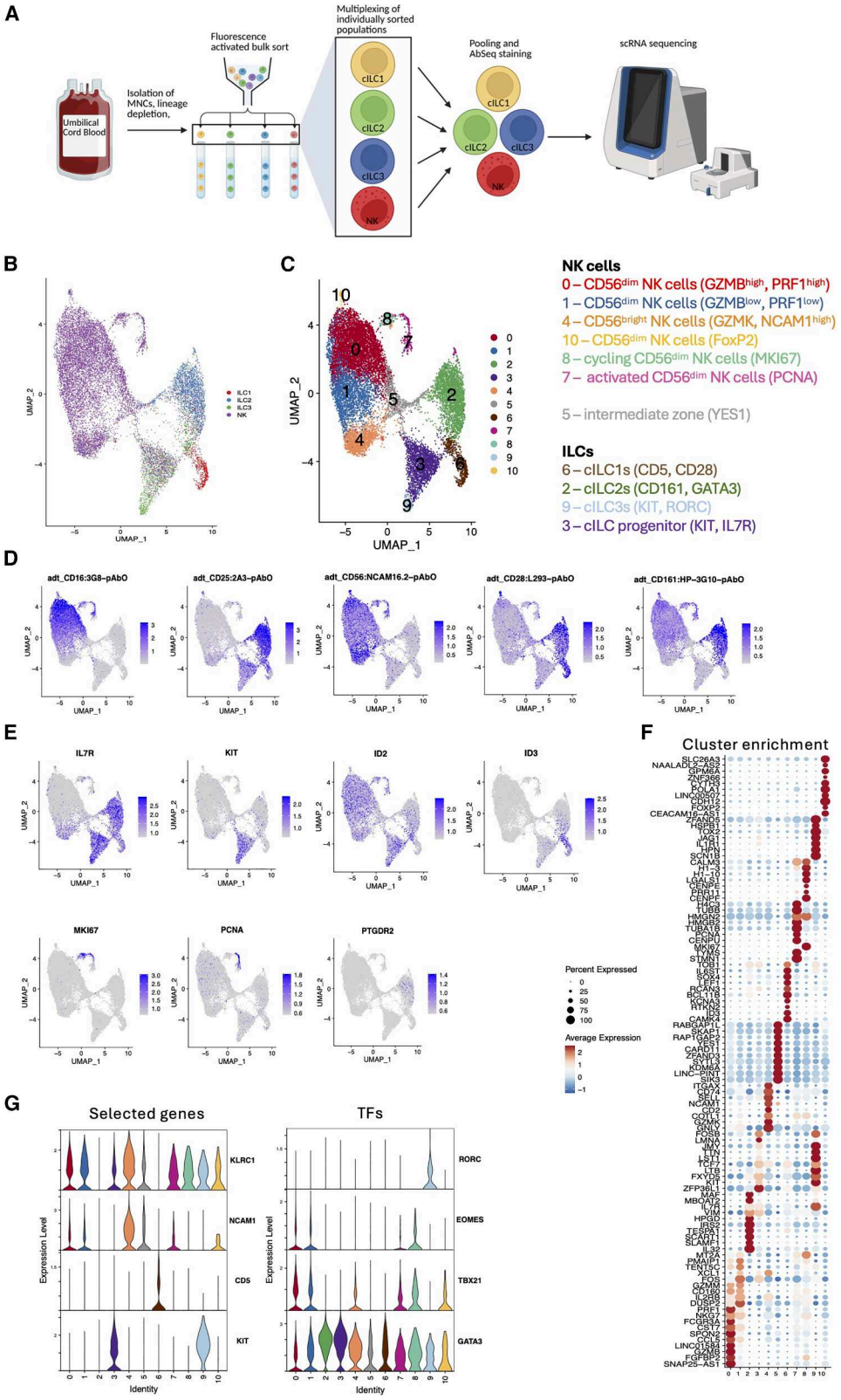

(legend on next page)

other hand, produced type 2 cytokines and remained stable in their phenotype.[15] Recently, a cytotoxic cILC2 subset was described within peripheral blood.[16]

cILC3s are identified as Lin$^-$CD94$^-$CD127$^+$CD117$^+$CRTH2$^-$ cells and, in contrast to tissue-resident ILC3s, are lacking NKp44 expression within the periphery except in certain conditions, such as inflammatory bowel disease.[3] A subset of cILC3s has been described as precursors to all three ILC subsets and NK cells.[6] Based on their KLRG1 and CD62L expression, peripheral blood cILC3s could be divided into three subsets showing divergent developmental potential, with one subset able to differentiate exclusively into ILC2s, one subset generating NK cells and ILC1s, and one subset able to develop into all three ILC subsets and NK cells.[17,18]

cILCs from CB are in a naive state and have not yet been shaped by the individual immunological history of a person. It is thus not surprising that cILCs go through substantial changes in their distribution and function throughout a lifetime. First of all, their overall frequencies decrease from the neonatal to the adult and elderly states, and total cILC cell numbers, in particular for cILC1s, are already decreasing from newborns to adolescents.[5,10,19] The factors that contribute to these age-related changes are poorly defined, but several studies suggest a multifactorial process influenced by infections,[20] autoimmune diseases,[21] exercise,[22,23] and nutrition.[24] Furthermore, cILC1–3s from CB exhibit a unique transcriptional profile compared to peripheral blood: they show a generally higher expression of the TF ID3 compared to adult cILC1–3s, while in the latter (and in tissue-resident ILCs), ID2 dominates.[7] Given the general importance of ID TFs for development of innate lymphocytes,[25,26] this suggests a functionally important switch from ID3 to ID2 from neonatal to post-birth ILCs.

Apart from ILC1–3s, also referred to as helper ILCs, natural killer (NK) cells, sometimes referred to as cytotoxic ILCs, have been categorized as part of the ILC family.[1] Circulating NK cells are classically divided into an abundant cytotoxic CD56^{dim} NK cell subset and a less abundant IFNγ-producing CD56^{bright} NK cell subset.[27] CD56^{dim} NK cells express granzyme B (GZMB) and perforin and vary in their expression of CD16, CD8, NKG2A, and killer-cell immunoglobulin-like receptors (KIRs).[28,29] CD56^{bright} NK cells, on the other hand, express NKG2A and granzyme K (GZMK) but lack CD16, CD8, and KIR surface expression.[29] Reminiscent of cILCs, CD56^{bright} NK cell frequencies and numbers are also highest in newborns and decrease with age.[19] It is also known that NK cell surface expression patterns change throughout a lifetime and acquire a more mature NK cell phenotype with increasing age.[30]

Transcriptional analysis by single-cell RNA-seq (scRNA-seq) has already been conducted for peripheral blood cILCs[4] and NK cells.[31,32] However, analyses of the transcriptional heterogenicity of CB cILCs and NK cells on the single-cell level are currently lacking. Here, to gain a deeper understanding of the underlying heterogeneity of CB cILCs, we sorted cILC1s, cILC2s, cILC3s, and NK cells by flow cytometry and performed scRNA-seq analyses. The study shows substantial intra-subset heterogeneity of cILC1s, cILC2s, cILC3s, and cILC progenitors (cILCps) and NK cells within CB. Moreover, we identified a previously unidentified cILC3 subset with selective responsiveness to CD28. Altogether, the present study utilizes scRNA-seq analyses to unravel the transcriptional heterogeneity of CB cILCs and NK cells leading to the definition of ILC subsets with characteristic phenotypic and functional properties and provides a versatile basis for further comparisons of neonatal cILCs with peripheral blood cILCs and tissue ILCs and NK cells in the future.

RESULTS

scRNA-seq reveals distinct transcriptional profiles for all three CB-derived cILC subsets, ILCps, and NK cells on the single-cell level

Previous transcriptomic analyses based on bulk RNA-seq showed a unique signature of each CB cILC subset with a distinct transcriptome compared to NK cells.[7] Despite their overall homogenous transcriptomic signatures, each CB cILC subset showed heterogeneous expression of extracellular surface receptors,[5,7] indicating further transcriptional heterogeneity within cILC subsets. To further explore this underlying heterogeneity, we performed scRNA-seq analyses of cILCs and NK cells from the CB of three donors (Figure 1A). First, cILC1s, cILC2s, cILC3s, and NK cells were individually cell sorted as described previously,[33] multiplexed with sample tag antibodies, and pooled. Subsequently, the pooled samples were labeled with a large Ab-Seq panel comprising 36 antibodies specific for various lineage antigens (Table S1). The uniform manifold approximation

Figure 1. Transcriptomic profiling of cord blood ILCs and NK cells by scRNA-seq

Mononuclear cells (MNCs) were isolated from fresh umbilical cord blood (CB) via a Ficoll gradient (n = 3). Unwanted cells were depleted using biotinylated antibodies (anti-CD3, anti-CD14, anti-CD19, and CD66b) and magnetic beads. The cells were stained to faithfully sort cILC1s (Lin$^-$CD94$^-$CD127$^+$CD117$^-$CRTH2$^-$), cILC2s (Lin$^-$CD94$^-$CD127$^+$CD117$^{-/+}$CRTH2$^+$), cILC3s (Lin$^-$CD94$^-$CD127$^+$CD117$^+$CRTH2$^-$), and NK cells (Lin$^-$CD94$^+$), as previously described.[5,7,33] The four individual populations were individually multiplexed, pooled, and stained with Ab-Seq antibodies.

(A) scRNA-seq was performed via the BD Rhapsody protocol.

(B and C) UMAP visualization of sorted populations (B) and individual clusters of CB cILCs and NK cells with color coding of the individual cluster 0–10. The following clusters were identified: 0, CD56^{dim} NK cells (*GZMB*^{high}); 1, CD56^{dim} NK cells (*GZMB*^{low}); 2, cILC2s (*GATA3*); 3, cILC progenitor (*KIT*); 4, CD56^{bright} NK cells (*GZMK*); 5, intermediate zone (NK/cILCs); 6, cILC1s (*CD5*); 7, activated CD56^{dim} NK cells (*PCNA*); 8, cycling CD56^{dim} NK cells (*MKI67*); 9, cILC3s (*RORC*); and 10, CD56^{dim} NK cells (*FOXP2*) (C).

(D and E) Feature plots showing CD16, CD25, CD56, CD28, and CD161 surface expression, respectively, determined by Ab-Seq antibodies (D) and the gene expression of the following selected genes: *IL7R*, *KIT*, *ID2*, *ID3*, *MKI67*, *PCNA*, and *PTGDR* (E).

(F) Dot plot showing the top 10 enriched genes within each cluster.

(G) Violin plots showing selected genes KLRC1, NCAM1, CD5, and KIT and transcription factors (TFs) GATA3, TBX21, EOMES, and RORC to identify the three cILC subsets and different NK cell subsets. The lineage (Lin) cocktail comprises the following antibodies: CD3, CD14, CD66b, CD1a, CD123, FcεR1, CD235a, TCRαβ, TCRγδ, and CD34.

and projection (UMAP) visualization of the scRNA-seq data clustered the cell mixture into two largely separate parts: a left lobe consisting of the sorted NK cell population and a right lobe predominantly containing the sorted cILC1–3 populations (Figure 1B). Within the NK cell population, three main clusters (0, 1, and 4) and several small satellite NK cell clusters (7, 8, and 10) were identified (Figure 1C), whereas the right lobe consisted of separate clusters for cILC1s (cluster 6), cILC2s (cluster 2), and cILC3s (clusters 3 and 9). The observed clusters showed inter-donor consistency (Figure S1A). Finally, there was a mixed cluster (cluster 5) incorporating cells with NK cell and ILC features at the contact zone between the NK cell and the ILC area. Calling of cell types was supported by Ab-Seq staining (Figure 1D), expression profiles of lineage-specific genes (Figures 1E and 1G), and cluster-specific gene enrichment analyses (Figure 1F) and validated using peripheral blood and tonsil ILC data from published scRNA-seq data by Jaeger et al.[11] (Figure S2).

cILC1s were localized in cluster 6 (Figure 1C), which encompassed cells exhibiting expression of *CD28*, *CD5*, and the TFs *ID3* and *SOX4* while lacking expression of the TF *ID2* and CD161 surface expression (Figures 1D–1F). These characteristics are compatible with previous analyses of cILC1s by bulk RNA-seq.[5,7,33] Notably, cILC1s were located at distance to the NK cell clusters within the UMAP analyses, suggesting a comparatively low degree of shared genes between these two functionally related innate lymphocyte types. Of note, Gene Ontology (GO) analyses revealed a small fraction of cILC1s that were associated with "positive T cell selection" and "thymic T cell selection" (Figure S3). cILC2s were mainly found in cluster 2 (Figure 1C) based on their expression of *CD25*, CD161, and *PTGDR2* (encoding CRTH2) and high expression of the TF *GATA3* (Figures 1D–1F). High expression of *KIT* (encoding CD117), representing an ILC3 feature, was found in two adjacent clusters (3 and 9) (Figures 1E–1G). cILC3s were identified in cluster 9 based on typical ILC3 features, characterized by high transcript levels of *IL1R1*, *KIT* (encoding *CD117*), and the TF *RORC*, respectively (Figures 1D–1G). The other, much larger cluster (cluster 3) did not show *RORC* expression and only moderate expression of *KIT* (CD117) but did show strong expression of *GATA3*, together pointing toward a putative ILCp population, as previously described.[6] This cluster also showed high CD25 expression (Figure 1D). cILC3s and putative cILCps (clusters 9 and 3) shared common pathways (GO terms) containing "activation," "adhesion," and "differentiation" (Figure S3).

NK cells were separated into six different clusters (clusters 0, 1, 4, 7, 8, and 10). Canonical CD56^{dim} NK cells could be annotated to cluster 0 by high expression of CD16 (*FCGR3A*), *GZMB*, and perforin (*PRF1*). CD56^{bright} NK cells were found in cluster 4 (Figure 1C), based on the highest CD56 (transcripts and Ab-Seq staining) and *GZMK* expression, while they lacked CD16 and CD8 (Figures 1D–1F). A subset located between canonical CD56^{bright} and CD56^{dim} NK cells (cluster 1) demarcated a transitional CD56^{dim} stage, characterized by low-level expression of GZMB and GZMK and intermediate expression of perforin. CD56^{bright} (cluster 4) and the main CD56^{dim} populations (clusters 0 and 1) exhibited an enrichment for genes related to IFNγ production (Figure S3). There were two more CD56^{dim} populations (clusters 7 and 8), which clustered apart from the main CD56^{dim} NK cell clusters and supposedly represent proliferating CD56^{dim} NK cells: cluster 7 was characterized by high expression of the proliferating cell nuclear antigen (*PCNA*) and cluster 8 showed strong expression of Ki-67 (*MKI67*), a marker for dividing cells (Figures 1E and 1F). In line with this, both clusters showed enriched pathways related to energy metabolism or chromosomal reorganization (Figure S3), suggesting that some NK cells in CB, although representing an immunologically naive source, are already in an activated and proliferating state. Cluster 10 contained an unusual population of CD56^{dim} NK cells that exhibited transcription of CD28 and *FOXP2* (Figures 1D and 1F), encoding the transcriptional repressor forkhead box protein 2. Finally, cluster 5 is located at the juncture between the two main NK cell and ILC lobes and constitutes an intermediate zone comprising cells with NK cell and cILC features. Trajectory analyses confirmed the intermediate state of this cluster (Figure S4A).

All in all, using our scRNA-seq data, we were able to faithfully identify CB cILC1s, cILC2s, cILC3s, putative cILCps, and several NK cell populations, including a FOXP2^{+} subset.

scRNA-seq of cILC1s revealed high heterogenicity based on CD5 and CD161 expression

As outlined above, our initial scRNA-seq analyses of cILC1s displayed a rather homogeneous signature (cluster 6, Figure 1C). However, we had previously shown that CB cILC1s could be further diversified on the basis of certain T cell-associated genes, such as CD5, and also contain a small CD161^{+} subset exhibiting ILC1-associated effector functions,[5,7] suggesting further heterogeneity. As we specifically sorted on cILC1s and labeled them with a unique tag (Figure 1A), we were able to recalculate clusters based on sorted cILC1s alone. This led to further diversification of cILC1s into seven clusters (Figure 2A), which were consistently observed in all three donors (Figure S1B).

Clusters 0 and 3 were characterized by the expression of T cell-associated genes (*CD5*, *CD6*, and *CCR7*), and both clusters showed enriched GO terms for "T cell differentiation in the thymus." This signature is reminiscent of thymic ILC1s (thyILC1s), an ILC1 population with NK cell differentiation potential that was recently described in the thymus.[14] Indeed, cILC1s show module score enrichment for published thyILC1 transcripts[14] (Figure S2E). This suggests that these two cILC1 subsets could be immature progenitors that recently emigrated from the thymus into CB. The two clusters could be separated by expression of the TF *SOX4* in a *SOX4^{high}* (cluster 3) and *SOX4^{low}* (cluster 0) subset (Figures 2B–2E). Since high *SOX4* expression is also a feature of thyILC1s,[14] cluster 3 might be in an earlier developmental state than cluster 0. Therefore, we calculated cell lineage trajectories by Slingshot analyses, which indeed suggests a differentiation path along a CD5/CD161 gradient from a putatively more immature CD5^{+}CD161^{-} cluster 3 to the more mature CD5^{-}CD161^{+} cluster 0 (Figure S4B).

The strong expression of *KLRB1*, encoding CD161, in clusters 1 and 2 (Figure 2B) is reminiscent of effector cILC1s of the CD161^{+}CD5^{-} phenotype, as recently shown in functional studies of CB-derived ILC1s.[5] In line with this, CD5 was only weakly expressed in cluster 1 and was completely absent in

CellPress
OPEN ACCESS

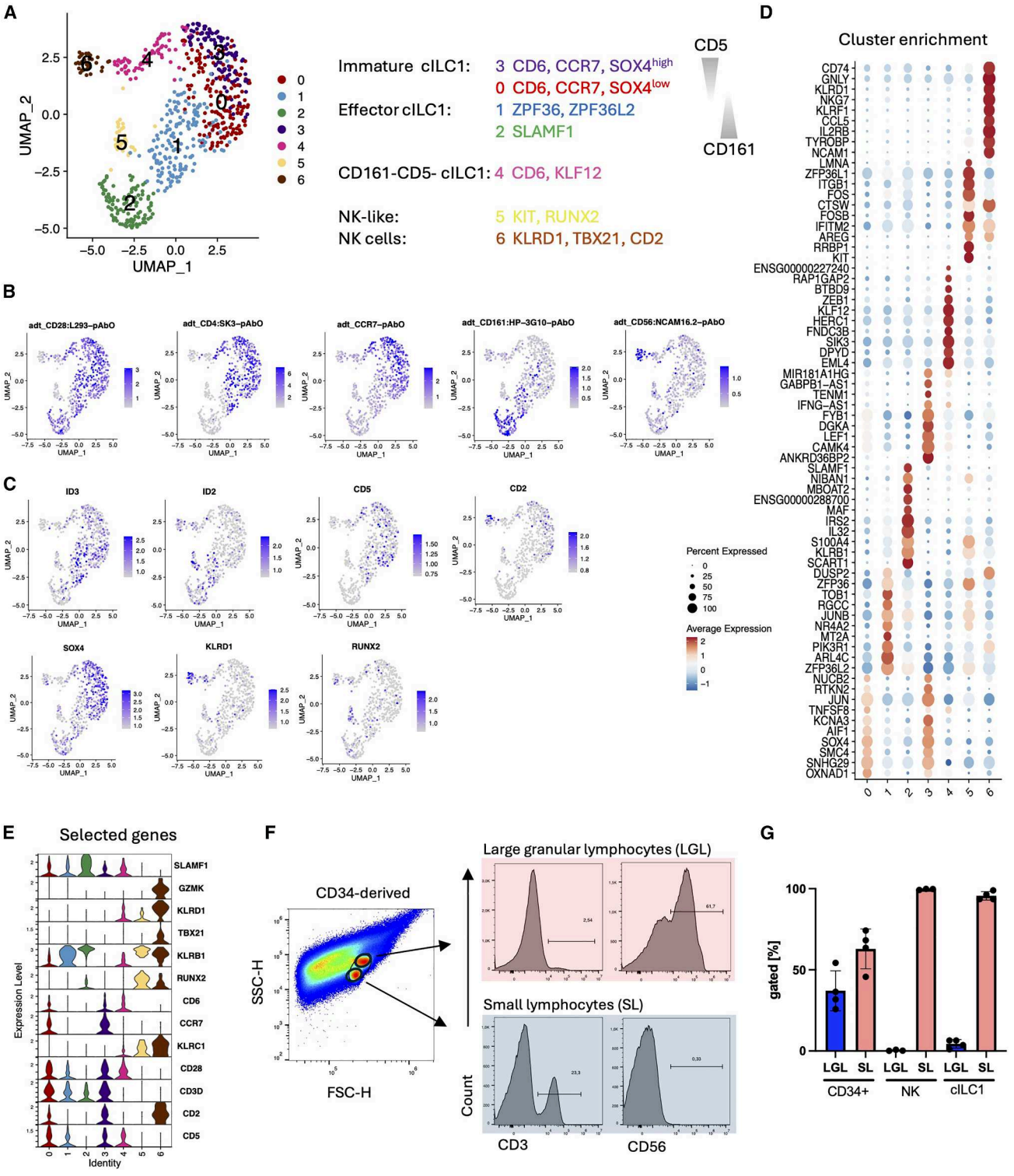

Figure 2. Transcriptomic heterogeneity of cILC1s based on CD5 and CD161 expression

The cILC1 subset was analyzed by scRNA-seq based on multiplexed labeling using the respective oligo-coupled sample tag antibodies.

(A) UMAP visualization of color-coded clusters 0–6 within the sorted cILC1s with annotation and schematic representation of reciprocal CD5 and CD161 gradients for clusters 0–3. The following clusters were identified: 0, immature cILC1s (*SOX4*^{low}); 1, effector cILC1s (*ZPF36*); 2, effector cILC1s (*SLAMF1*); 3, immature cILC1s (*SOX4*^{high}); 4, CD5^{-}CD161^{-} cILC1 (*KLF12*); 5, NK-like (*RUNX2*); and 6, NK cells (*KLRD1*).

(legend continued on next page)

cluster 2. cILC1s in cluster 1 were distinguished from those of cluster 2 by expression of the zinc finger ring proteins *ZFP36* and *ZFP36L2*, which are both involved in negative regulation of inflammatory responses by promoting mRNA decay mechanisms, whereas cILC1s in cluster 2 showed selective expression of signaling lymphocytic activation molecule 1 (*SLAMF1/CD150*) (Figures 2D and 2E). We previously showed, using bulk RNA-seq analysis, that the co-stimulatory molecule SLAMF1 is indeed expressed in cILC1s (as well as cILC2s, cILC3s, and T cells) from CB but not NK cells.[7] Furthermore, pathway analyses revealed an enrichment of transcripts associated with IFNγ production in cluster 1 (Figure S3B), which, together with SLAMF1 expression, is again compatible with the suggested effector state of this subset.

The focused scRNA-seq analysis also identified a cILC1 subset that expressed neither CD5 nor CD161 (cluster 4). Instead, this cluster exhibited moderate expression of the NK cell marker CD94 and selectively expressed the TF *KLF12* (Figures 2B–2E), which was previously shown to be involved in NK cell maturation and proliferation in mice.[34] Cluster 4 likely demarcates an intermediate subset located between immature cILC1s in cluster 3 and a subset with clear NK cell characteristics in cluster 6. In fact, the expression of GZMK, an early granzyme associated with CD56^{bright} NK cells, and *KLRF1* (NKp80), whose expression is largely restricted to NK cells, suggests that cells in cluster 6 might indeed represent CD56^{bright} NK cells. Finally, cluster 5 is separated from the other clusters and is enriched for cells expressing *KLRB1* (CD161), *KIT* (encoding CD117), and *RUNX2*, an early TF involved in NK cell development, pointing toward a progenitor state with an ILC1-associated phenotype (Figures 2B–2E). Altogether, the focused scRNA-seq analysis of cILC1s revealed substantial heterogeneity within the human cILC1 compartment, with distinct subpopulations representing different maturation states from early cILC1s, probably representing recent emigrants from the thymus (clusters 0 and 3), to more mature cILC1s (clusters 1 and 2) based on differential CD5 and CD161 expression. Furthermore, we could identify several subsets that exhibit NK cell features, including a *KLF12*-expressing subset (cluster 4) and a *RUNX2*-expressing putative NK cell progenitor (cluster 5).

cILC1s have differentiation potential toward NK cells but not T cells

We previously demonstrated that cILC1s have NK cell differentiation potential with a bias toward the generation of KIR$^+$NKG2A$^-$ NK cells, a subset that is not efficiently generated from other previously defined NK cell precursors.[5] More recently, we identified a putative precursor of cILC1s, termed thyILC1s, in the thymus of small children that exhibits close transcriptional similarity to thymic CD34$^+$CD4$^-$CD8$^-$ double-negative (DN) cells, constituting an early T cell progenitor subset.[14] These observations prompted us to explore whether cILC1s have residual T cell differentiation potential. To this end, we exploited a 3D artificial thymic organoid (ATO) model, which was previously shown to faithfully support the development of CD3$^+$TCRαβ T cells from hematopoietic stem and progenitor cells (HSPCs).[35] We thus isolated three different cell types, namely HSPCs (CD34$^+$Lin$^-$CD94$^-$), cILC1s (Lin$^-$CD34$^-$CD94$^-$CD127$^+$CD117$^-$CRTH2$^-$), and CD56^{bright} NK cells (Lin$^-$CD34$^-$CD94$^+$CD127$^+$), from CB by flow cytometric cell sorting and co-cultured them in the ATO model for 4 weeks.

As expected, the HSPCs differentiated into two distinct populations, which could be identified based on their size (forward scatter [FSC]) and their granularity (side scatter [SSC]) as large granular lymphocytes (LGLs) and small lymphocytes (SLs) (Figure 2F). The LGLs exhibited the typical NK cell surface phenotype (CD3$^-$CD56$^+$), while a subset of SLs were identified as T cells based on their CD3$^+$CD56$^-$ phenotype (Figure 2F). The *de-novo*-generated T cells were predominantly TCRαβ, with a minor TCRγδ subset (Figure S5). As expected, whereas CD34$^+$ HSPCs showed potential toward both NK and T cells, sorted NK cells remained stable in the ATO model and did not show any CD3 expression (Figure 2G). Importantly, cILC1s selectively differentiated into CD3$^-$CD56$^+$ NK cells but not CD3$^+$CD56$^-$ T cells (Figure 2G). Thus, although transcriptionally closely related to T cells, neonatal cILC1s are unable to realize a T cell fate but still have NK cell differentiation potential.

Identification of four cILC2 subsets using scRNA-seq

cILC2s are supposedly the best-characterized cILC subset, due to their phenotypic and functional similarities to tissue-resident ILC2s and their well-documented involvement in clinically relevant settings, such as aggravating allergic reactions.[2,3] To determine the heterogeneity of CB cILC2s, we performed a focused scRNA-seq analysis of cILC2s (cluster 2, Figures 1B and 1C), as described above for cILC1s, leading to the identification of six separate clusters (Figure 3A). The clusters showed inter-donor consistency. However, one donor had a low frequency of cILC2s (Figure S1C).

The first three cILC2 clusters (0, 1, and 2) are closely related and share expression of cILC2 signature genes, including CD161 (*KLRB1*), *CD25*, *PTGDR2* (CRTH2), and *KLRG1* and

(B and C) Feature plots showing CD28, CD4, CCR7, CD161, and CD56 surface expression determined by Ab-Seq antibodies (B) and the gene expression of selected genes: *ID3*, *ID2*, *CD5*, *CD2*, *SOX4*, *KLRD1*, and *RUNX2* (C).

(D) Dot plot showing the top 10 enriched genes within each cluster.

(E) Violin plots showing selected genes SLAMF1, *KLRD1*, *TBX21*, *CCR7*, *KLRB1*, *KLRC1*, *RUNX2*, *CD28*, *CD5*, *GZMK*, *CD2*, and *CD3D* to identify different cILC1 subpopulations. Fresh cord blood MNCs were enriched as described in Figure 1 and subsequently sorted as CB CD34$^+$ (Lin$^-$CD34$^+$), cILC1s (Lin$^-$CD34$^-$CD94$^-$CD127$^+$CD117$^-$CRTH2$^-$), and NK cells (Lin$^-$CD34$^-$CD94$^+$CD127$^+$) (n = 3–4). Individual populations were mixed with the murine cell line MS5-hDLL1, cultivated for 29 days, and analyzed via flow cytometry.

(F) The exemplary dot plot for forward scatter (FSC-H) and side scatter (SSC-H) is shown from one CD34-derived culture. Two populations were identified according to their size and granularity into large granular lymphocytes (LGLs) and small lymphocytes (SLs). Exemplary histograms show CD3 and CD56 expression for LGLs (top line) and SLs (bottom line).

(G) Bar graphs showing the percental distributions of LGLs (blue bar) and SLs (red bar) from CD34$^+$ cells, NK cells, and cILC1s. The heights of the bars represent the mean ± SEM.

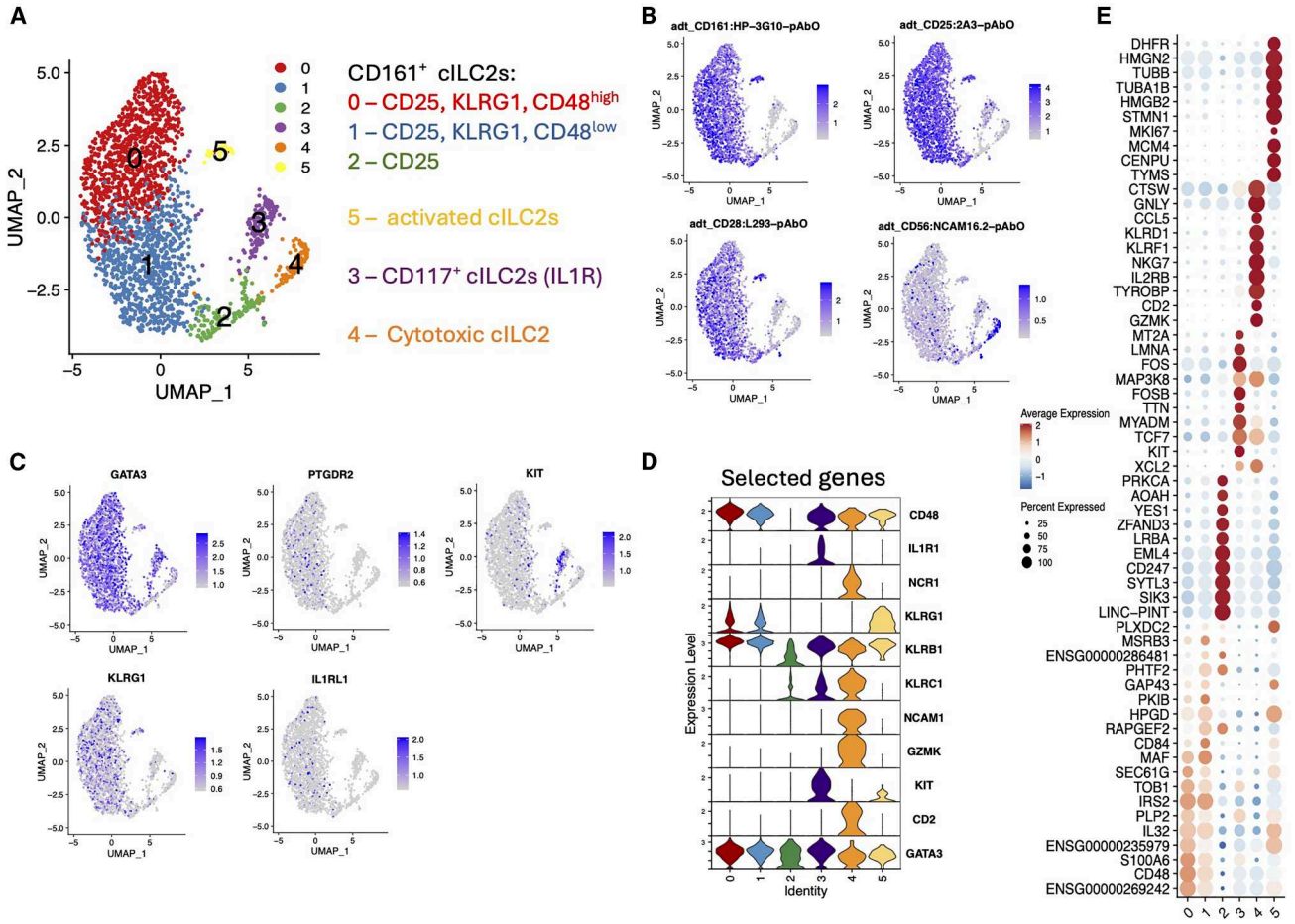

Figure 3. Identification of CD117^{-}, CD117^{+}, activated, and cytotoxic cILC2s by scRNA-seq

The cILC2 subset was analyzed by scRNA-seq based on multiplexed labeling using the respective oligo-coupled sample tag antibodies. A

(A) UMAP visualization of color-coded clusters 0–5 within the sorted cILC2s with subset annotation. The following clusters were identified: 0, CD161^{+} cILC2s (CD48^{high}); 1, CD161^{+} cILC2 (CD48^{low}); 2, CD161^{+} cILC2 (*CD25*); 3, CD117^{+} cILC2 (*IL1R*); 4, cytotoxic cILC2s (*GZMK*); and 5, activated cILC2s (*MKI67*) (A).

(B and C) Feature plots showing CD161, CD25, CD28, and CD56 surface expression determined by Ab-Seq antibodies (B) and the gene expression of selected genes: *GATA3*, *PTGDR2* (CRTH2), *KIT* (CD117), *KLRG1*, and *IL1RL1* (C).

(D) Violin plots showing selected genes *CD48*, *IL1R1*, *NCR1*, *KLRG1*, *KLRB1*, *KLRC1*, *NCAM1*, *GZMK*, *KIT*, *CD2*, and *GATA3* to identify different cILC2 subpopulations.

(E) Dot plot showing the top 10 enriched genes within each cluster.

moderate expression of *IL1RL1* (encoding the IL-33 receptor) and *GATA3^{high}* but low levels of *KIT* (CD117) expression (Figures 3B–3E). Together, the three clusters (0–2) constitute the canonical CD117^{-} cILC2 subset. We next tried to distinguish the canonical ILC2 clusters on the basis of CD48 expression, which was highest in cluster 0 and lowest in cluster 2 (Figures 3D and 3E). Notably, engagement of CD48 via CD244 (2B4) has previously been proposed to promote human ILC2 differentiation.[36] However, this did not translate into notably different levels of CD48 surface expression by flow cytometry (Figure S6).

Another CD117^{-} cILC2 subset, comprising activated and dividing cells, is located in cluster 5 and is characterized by strong expression of Ki67 (*MKI67*) and corresponding enriched GO terms (Figures 3E and S3C). CD117^{+} cILC2s were found to be enriched in cluster 3 and could be further characterized by expression of *IL1R* and gene enrichment in pathways involved in IFNγ production (Figures 3C and S3C). Finally, a putative cytotoxic subset was identified in cluster 4 due to the enrichment of genes typically associated with NK cells (*GZMK*, KLRC1 [encoding NKG2A], CD56/*NCAM1*, *KLRD1* [encoding CD94], and *KLRF1* [encoding NKp80]), *CD2*, and enriched pathways for IFNγ production (Figures 3B–3E and S3C). To further substantiate the identity of cluster 4, we performed cytoplasmic staining for GZMK and could clearly distinguish a small subset of CRTH2^{+} cILC2s that expressed GZMK at comparable amounts to CD56^{bright} NK cells (mean frequency: 7.8%, *n* = 5; Figure S6). Together, scRNA-seq analyses revealed four clearly distinguishable cILC2 subsets within human CB: a major CD117^{-} subset distributed over three clusters with minor transcriptional differences based on CD48 expression, which could represent different maturation states among canonical cILC2s;

a KI67$^+$ subset representing activated cILC2s; a CD117$^+$ cILC2 subset; and finally, a putatively cytotoxic cILC2 subset.

scRNA-seq reveals distinct subsets within CB cILC3s

CB cILC3s have been described to have dual roles: on the one hand, they constitute ILCps,[6] and on the other hand, they are effector cells that can be triggered by innate stimuli such as Toll-like receptor (TLR) ligands.[7] This opens the possibility that cILC3s comprise several subpopulations with different functional properties. Using the sorting strategy commonly used to define cILC3s,[33] we identified four cILC3 subsets and one NK cell subset by scRNA-seq (Figure 4A), which was consistent for all three donors (Figure S1D). *KIT*, encoding the ILC3 marker CD117, was found to be highly expressed in the two adjacent clusters (0 and 1). Cluster 0 was enriched for CD25$^+$ cells and high *SELL* expression, encoding CD62L (Figures 4C and 4D), compatible with the previously defined phenotype of ILCps,[6,17,37] whereas the adjacent cluster 1 contained canonical *RORC*$^+$*IL1R1*$^+$ cILC3s (Figures 4B–4D). We validated this annotation using a published dataset of tonsillar ILC3s by Jaeger et al.[11] with Module Score enrichment (Figure S2F).

CD161$^+$ cILC3s were identified in cluster 2, which showed high co-expression of CD28, accompanied by lower *KIT* transcripts, compared to clusters 0 and 1 (Figures 4B–4D). Since KLRG1 is prominently expressed on cILC2s (Figure 3), we mapped the KLRG1$^+$ cILC3s (cluster 2) onto the global UMAP (Figures 1B and 1C). As expected, cluster 2 was located within the cILC3 cluster (Figure S2G). The two small clusters, 3 and 4, both expressed *RUNX2* and the NK cell receptors *KLRC1* (NKG2A) and *KLRD1* (CD94). We annotated cluster 3 as residual CD56^{bright} NK cells due to the typical NK cell signature (*CD2*, *GZMK*, *NCAM1*, *NCR1* [NKp46], and *KLRF1* [NKp80]) and presence of enriched "cytotoxic" pathways (Figures 4B–4D and S3D). In contrast, cluster 4 did not express CD56 on the cell surface and had rather low *KLRD1* transcript levels, which could point toward an NK cell progenitor but is also reminiscent of exhausted NK cells (Figures 4B–4D). All in all, we could distinguish four subsets within cILC3s by scRNA-seq analyses, corresponding to canonical cILC3s (CD28$^-$CD25$^-$CD161^{low}CD56$^-$CD117^{high}), cILCps (CD28$^-$CD25$^+$CD161^{low}CD56$^-$CD117^{high}CD62L$^+$), a CD28$^+$ cILC3 subset (CD28$^+$CD117^{low}CD161^{high}KLRG1$^+$), and finally, a subset combining ILC3 and NK cell features, termed pre-NK cILC3s.

CD28$^+$CD161$^+$ cILC3s exert type 1 effector functions upon stimulation with a CD28 superagonist and IL-2

As mentioned above, we identified a CD28$^+$CD161$^+$ cILC3 subset (cluster 2) with low expression of *KIT* (Figure 4A). Flow cytometric staining of cILC3s indeed revealed a distinct CD28$^+$ cILC3 population exhibiting significantly lower CD117 expression but higher CD161 expression (both based on mean fluorescence intensity [MFI]) compared to CD28$^-$ cILC3s (Figure 4E). Thus, cILC3s can be further subdivided based on differential surface expression of CD28. Since engagement of CD28 provides a second signal for activation of naive T cells, we were wondering if CD28$^+$ cILC3s can be similarly activated by engagement of CD28 ligands. To this end, we stimulated flow cytometrically sorted cILC3s with a CD28 superagonist antibody and analyzed the cytokine production capacity of CD28$^+$ cILC3s with or without IL-2. Notably, there was no induction of the typical cILC3 effector cytokines IL-22 or IL-17A, nor TNF-α, in any of the conditions (Figure S7). However, we observed a significant induction of IFNγ production in CD28$^+$CD161$^+$ cILC3s following stimulation with the CD28 superagonist in combination with IL-2 (Figure 4F). Neither IL-2 nor the CD28 superagonist alone led to any appreciable IFNγ production.

Finally, in order to find out if, similar to T cells, CD28 expression on cILC3s decreases with age, we took advantage of a dataset from a previous study of cILC3 frequencies in infants and adolescents.[19] Unexpectedly, we found an age-related increase of the CD28$^+$ cILC3 effector subset, with CB showing the lowest values compared to children of all age groups and, in particular, a significant increase toward adolescents (13–18 years) (Figure S8).

DISCUSSION

The present study provides a thorough analysis of the transcriptional landscape of innate lymphocytes in neonates on the single-cell level. The established lymphoid cell types cILC1–3s and NK cells were readily identified in the CB of healthy babies. Moreover, within each cell type, multiple subsets could be identified on the basis of scRNA-seq data and functional analysis.

ILC1s are the least-well-characterized ILC subset, not only in the circulation but also in tissues, due to the absence of unique "ILC1-inclusion markers." Our scRNA-seq analyses confirm previous analyses that the majority of cILC1s can be classified according to their CD5 and CD161 expression, with a dominant CD5$^+$ cILC1 fraction.[5,7] In a recent study of thyILCs, we suggested that CD5$^+$ thyILC1s might directly egress from the human thymus to become cILC1s in peripheral blood and eventually develop into effector cILC1s by upregulation of CD161.[5] Indeed, UMAP visualization indicates a gradient from immature CD5$^+$ cILC1s toward effector CD161$^+$ cILC1s and finally NK-like cILC1s. This relationship was also suggested by trajectory analyses. This is also in line with our previous observation that the frequency of CD5$^+$ cILC1s decreased significantly, while the frequency of CD5$^+$CD161$^+$ cILC1s significantly increased from newborns to adolescence.[19] This suggests an adaptation of cILC1s toward a more mature state with increasing age, which might be linked to higher functionality. Furthermore, immature CD5$^+$ cILC1s showed enriched GO terms related to "T cell selection" and "T cell development," suggesting a developmental route shared with early T cell stages in the thymus. Along those lines, immature CD5$^+$ cILC1s also expressed the TF *SOX4,* which is strongly expressed on thymic T cell progenitors,[38] and we also recently observed high *SOX4* expression on CD5$^+$ thyILC1s.[14] Notably, in that study, we observed a significant decrease in peripheral blood cILC1s in pediatric patients with known inborn errors affecting the thymic architecture, further suggesting a thymic origin of cILC1s.[14] In the present study, the effector cILC1 subset that expressed CD5 and CD161 (cluster 1) showed enriched *ZPF36* and *ZPF36L2* transcripts. In murine T cells, ZPF36L2 has been described to be required for antigen-specific T cell clonal expansion and T cell priming.[39] The role of ZPF36L2 in cILC1s needs to be investigated; however, it might be an

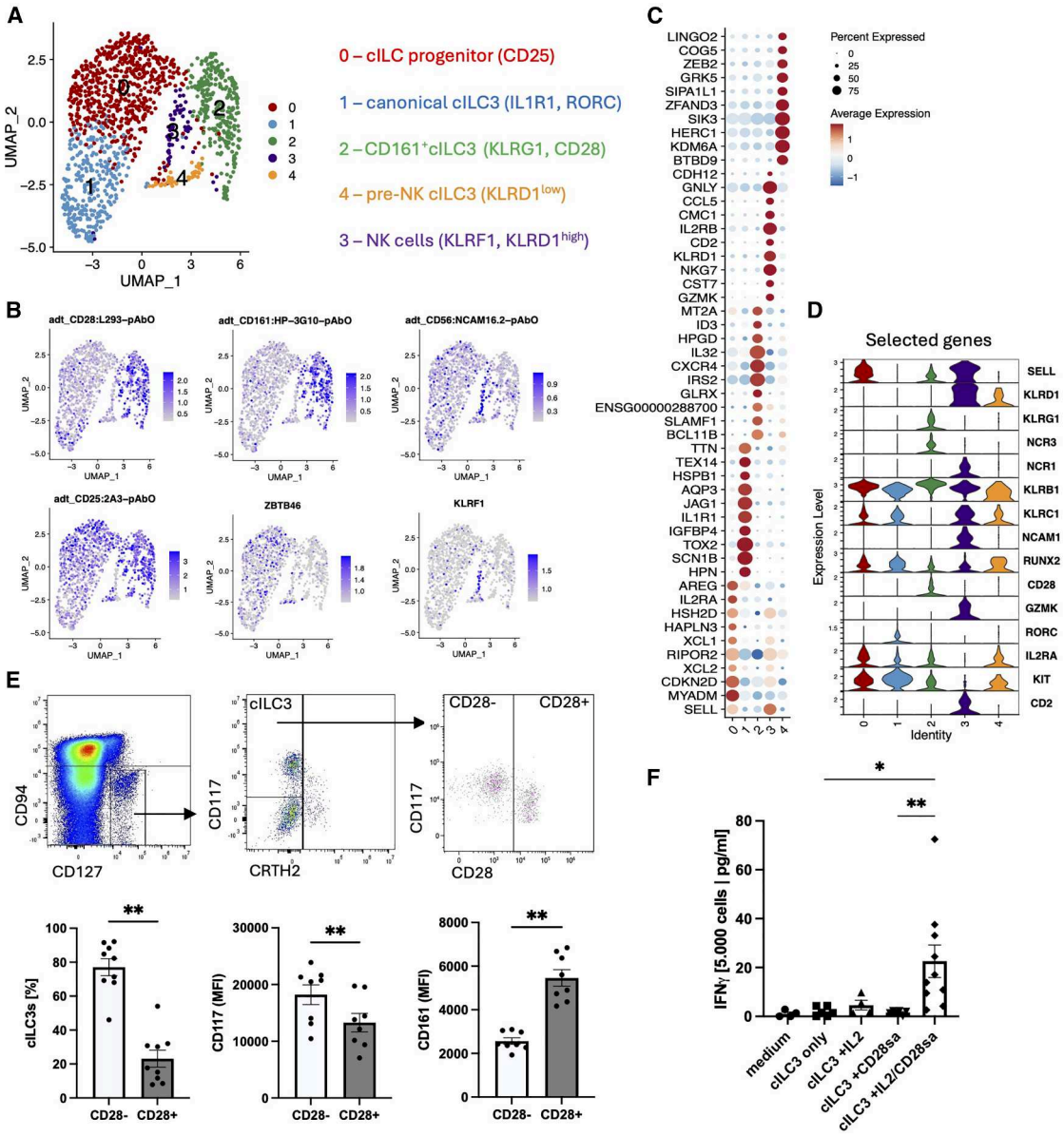

Figure 4. A CD28^{+}CD161^{+}CD117^{low} cILC3 subset that is responsive to a CD28 superagonist

The cILC3 subset was analyzed by scRNA-seq based on multiplexed labeling using the respective oligo-coupled sample tag antibodies.

(A) UMAP visualization of color-coded clusters 0–4 within the sorted cILC3s with subset annotation. The following clusters were identified: 0, cILC progenitor (*CD25*); 1, canonical cILC3 (RORC); 2, CD161^{+} cILC3 (CD28); 3, NK cells (KLRD1^{low}); and 4, pre-NK cells (KLRD1^{high}).

(B) Feature plots showing CD28, CD161, CD56, CD25, and CD62L surface expression determined by Ab-Seq antibodies and the gene expression of selected genes: *ZBTB46* and *KLRF1*.

(C) Dot plot showing the top 10 enriched genes within each cluster.

(D) Violin plots showing selected genes *SELL*, *KLRD1*, *KLRG1*, *NCR3*, *NCR1*, *NCAM1*, *RUNX2*, *CD28*, *GZMK*, *RORC*, *IL12RA*, *KIT*, *KIT*, and *CD2* to identify different cILC3 subpopulations. Mononuclear cells were freshly isolated and analyzed via flow cytometry. Exemplary dot plots show the used gating strategy: cILCs were identified by CD127 expression and gating out CD94. cILC3s were identified as CD117^{+}CRTH2^{-} cells.

(E) Exemplary dot plot shows CD28 and CD117 expression with quantification of CD28 frequencies of cILC3s and the mean fluorescence intensity (MFI) of CD117 and CD161 between CD28^{+} and CD28^{-} cILC3s (n = 8–9). Sorted cILC3s were stimulated for 5 days in medium alone, CD28 superagonist alone, IL-2 alone, or CD28 superagonist plus IL-2.

(F) Bar graphs show IFNγ secretion from the different conditions (n = 4–9). The heights of the bars represent the mean ± SEM.

(E and F) The levels of significance were calculated using a Wilcoxon test (E) and a non-parametric ANOVA (Kruskal-Wallis test) with Dunn's multiple comparison test (F). *p < 0.05 and **p < 0.01.

indication of a specific clonal expansion of cILC1s. All in all, these results strengthen a model in which potential CD5$^+$ cILC1s originate within the human thymus and egress into the periphery in a process involving upregulation of CD161 and, eventually, downregulation of CD5.

We recently demonstrated the ability of cILC1s and thyILC1s to differentiate into KIR$^+$ NK cells using the murine feeder cell line OP9-DLL1.[5,14] Both CD5$^+$ and CD5$^-$ cILC1s differentiated into KIR$^+$ NK cells in bulk and single-cell cloning experiments.[5] In contrast, they did not differentiate into T cells using an established T cell differentiation protocol,[40,41] although a recent study suggested that cILC1-like cells from peripheral blood could develop into T cells using a PHA-based stimulation protocol.[11] To determine their differentiation potential toward T cells, we utilized an advanced thymic differentiation model (ATO model).[35] Again, cILCs were not able to realize a T cell fate, while efficient differentiation into NK cells was observed. Notably, we identified two ILC1 subsets that expressed TFs associated with NK cell development: one subset expressing *RUNX2* (cluster 5) that was previously shown to promote early stages of NK cell development[42] and another subset expressing *KLF12* (cluster 4), a TF promoting increased proliferation at later stages of NK cell development.[34] In the UMAP projection focusing on cILC1s (Figure 2A), the *KLF12* subset is bridging the main cILC1 subsets with residual CD56^{bright} NK cells (cluster 6), again indicative of an intermediate differentiation state of this subset. Nevertheless, canonical cILC1s and NK cells clearly cluster apart from each other in the main UMAP plots (Figure 1C), and cILC1s are generally more closely related to T cells (in particular CD4$^+$ T cells) than NK cells, as shown in previous transcriptomic analyses.[7] This close transcriptional similarity to T cells might well be related to a thymic origin of the neonatal cILC1s,[14] as discussed above. In line with this, we observed a significant decrease in cILC1s in FOXN1^{het} patients and patients with thymic aplasia (complete DiGeorge syndrome) compared to age-matched reference values,[14] strengthening the assumption of a thymic origin of cILC1s.

Six cILC2 subsets could be distinguished in our scRNA-seq data. Four subsets had the canonical CD117$^-$ phenotype, expressing high levels of *GATA3*, CD161, *IL1RL1* (encoding IL-33R), *CD48*, *CD28*, *KLRG1*, and *CD25*, very similar to peripheral blood and tissue ILC2s.[4,8] Three of the CD117$^-$ cILC2 subsets could be further distinguished by different levels of CD48 expression, which was recently suggested to be involved in promoting cILC2 differentiation.[36] However, when analyzed by flow cytometry, the transcriptional differences in CD48 were not apparent on the cell surface, and it remains unclear if the transcriptional differences between the three canonical ILC2 subsets indeed reflect different maturation stages of cILC2s. A fourth CD117$^-$ subset expressing Ki67 likely represented proliferating ILC2s. CD117$^+$ cILC2s displayed transcripts for *IL1R* and *IFNG*, which is in line with their described ability to secrete either ILC3-associated cytokines or ILC1-associated cytokines depending on the stimulus.[15] Based on our scRNA-seq data, CD117$^+$ cILC2s hardly expressed *KLRG1*, *CD28*, and *PTGDR2* (encoding CRTH2) transcripts. Finally, we could identify a putatively cytotoxic CD56$^+$ cILC2 subset in CB, exhibiting transcription of *GZMK*. We confirmed the presence of a GZMK$^+$ cILC2 subset in CB by flow cytometry, with an average of 7.8%. Notably, a recent study identified cytotoxic cILC2s in peripheral blood expressing GZMB.[16] This suggests a more immature stage of cytotoxic cILC2s in CB compared to peripheral blood, which would mirror GZMK and GZMB expression in CD56^{bright} and CD56^{dim} NK cells, respectively.[43] The potential functionality of this subset in CB needs to be determined by future studies.

Lin$^-$CD127$^+$CD94$^-$CD117$^+$ cILC3s have been described to be ILCps[6,17] but, at the same time, have effector functionality when stimulated with TLR2:1 ligands.[3] So far, it was unknown if cILC3s combine both functionalities or if this might be attributed to different subsets of cILC3s.[3] Our scRNA-seq data identified four different cILC3 subsets in CB. Canonical cILC3s were identified as CD28$^-$CD25$^-$CD161^{low}CD56$^-$CD117^{high} and moderately expressed *RORC* transcripts. In contrast to canonical cILC3s, the putative ILCp subset showed CD25 and *SELL* (CD62L) expression (CD28$^-$CD25$^+$CD161^{low}CD56$^-$CD117-^{high}CD62L$^+$), similar to the CD62L$^+$ ILC3-like progenitors previously defined in peripheral blood and human tissues.[17,44] Although we did not confirm their progenitor functionality, the present data suggest that ILCps constitute a separate subset distinct from other subsets of conventional cILC3s with effector functions.

Furthermore, we identified a CD28-expressing cILC3 subset (CD28$^+$CD117^{low}CD161^{high}KLRG1$^+$), with high CD161 and low *KIT* (CD117) expression, based on our scRNA-seq analyses and flow cytometry. Upon stimulation with a CD28 superagonist and IL-2, cILC3s secreted IFNγ but not the ILC3 signature cytokines IL-22 and IL-17a. This might be due to divergent intracellular mechanisms after CD28 superagonist stimulation. CD28 stimulation directly affects the activation of vital TFs, such as NFAT, AP1, MYC, FOC, JUN, and nuclear factor κB (NF-κB).[45] In this regard, CD28 superagonist stimulation can induce IFNγ secretion in murine T_H1 cells.[46] On the other hand, IL-22 and IL-17A secretion is dependent on AhR, RORC,[47,48] and mTOR complex 1.[49] Of note, we have previously reported that cILC3s were able to secrete IFNγ after TLR2:1 ligand stimulation, whereas they remained unable to secrete IL-17A and IL-22 even after specific interleukin stimulation.[6,7] Together, the present findings suggest that neonatal cILC3s are more prone toward type I cytokine secretion than tissue-resident ILC3s and that cILC3s and tILC3s are generally not functionally equivalent. Furthermore, the question arises whether CD28-mediated stimulation of cILC3 *in vivo* is dependent on cytokine-mediated co-signaling (here, IL-2) or on interaction with dendritic cells via CD80/CD86, or whether alternative receptor-mediated signals, similar to T cells,[50] exist. Furthermore, we observed a significant increase in CD28$^+$ cILC3s from CB to adolescents (13–18 years), which might reflect the gain of immunological experience during aging. Of note, this is in contrast to T cells, where CD28 expression is preferentially found on naive T cells and is lost upon activation, accompanied by a well-described age-related decrease of CD28$^+$ T cells.[51] This contrast in CD28 functionality between ILCs and T cells needs to be further investigated. Of note, CD28 expression is also found on cILC2 and cILC1s,[5,7] indicating that all three cILC subsets might receive functional activation cues via alternative stimulation signals.

Finally, the majority of CB NK cells identified by scRNA-seq could be attributed to the well-defined CD56^{dim} and CD56^{bright} subsets. Interestingly, besides the canonical CD56^{dim} subset with high expression of CD16 and cytotoxic molecules, another sizable CD56^{dim} subset was identified with intermediate characteristics between canonical CD56^{dim} and CD56^{bright} NK cells. This subset (cluster 1) is characterized by low expression of CD16 and low-level expression of both *GZMB* and *GZMK*, the latter constituting a hallmark of CD56^{bright} NK cells. This finding is in line with a model of NK cell differentiation, which sees CD56^{bright} NK cells as progenitors of CD56^{dim} effector NK cells, but definitive proof of this concept is still missing.[29] This subset defined here in CB might help to experimentally clarify the relationship between the two major NK cell subsets. Besides two clearly demarcated subsets identifying activated and proliferating NK cells, scRNA-seq analysis revealed a small subset of FoxP2-expressing NK cells, a TF that, to our knowledge, has so far not been reported in primary NK cells (Figures 1D and 1F) but was found to be expressed in NK cell lines such as NK92 and YT.[52] Moreover, FoxP2 was recently reported to regulate differentiation of the inflammatory T helper cell subset 9 (Th9 cells).[53] Together, these findings merit further investigation of the functional role of this unusual NK cell subset.

In summary, the present scRNA-seq-based analysis of CB cILCs and NK cells provides a versatile resource with which to deeply dig into the heterogeneity of ILCs in newborns and enables further comparison with the respective scRNA-seq datasets available from human tissues and peripheral blood. We confirmed the presence of the main canonical cILC and NK cell subsets in CB but also identified subsets due to the discriminatory power of scRNA-seq analysis in combination with a large Ab-Seq panel. Given the naive state of CB, it was surprising to identify NK cell and cILC2 subsets with expression signatures of activated and proliferating cells. It will be interesting to see if the time of delivery, either preterm, term, or late term, will correlate with the size of the activated clusters, which could point toward either early homeostatic proliferation or activation by yet unknown stimuli. Furthermore, the present data, together with published scRNA-seq data from thyILC1s,[14] strengthen the idea that neonatal cILC1s have a thymic origin. Finally, we have identified a CD28^{+} cILC3 subset that can be stimulated with a CD28 superagonist, a property that was thought to be an exclusive feature of T cells. Given that CD28 is also expressed on cILC1 and cILC2 subsets, this finding is particularly relevant with regard to future clinical use of cILCs in novel therapeutic approaches.

Limitations of the study

Although the present study provides a thorough account of ILC diversity in umbilical CB on the single-cell level, the approach relied on cell populations that were flow cytometrically sorted on the basis of surface markers. A holistic approach considering the whole, unbiased diversity of cell types could putatively capture cells that have evaded our sorting approach. However, considering that ILC1–3s together typically account for less than 1% of lymphocytes, our enrichment strategy enabled a thorough display of cell diversity within the boundaries of the basic cILC subtypes. It needs to be mentioned that this approach might bear the potential of introducing contaminating cells from other lineages due to the sorting process. Hence, called individual cILC subpopulations, which were not validated based on flow cytometry, need to be treated with caution and validated in further studies. Another limitation concerns the significance of the CD28-based activation of cILC3. It is currently unclear if superagonistic stimulation via CD28 is occurring *in vivo*, for example, in the context of an immune synapse involving antigen-presenting cells, or if the stimulus is indeed artificial. Furthermore, the clinical relevance of such an induced stimulation of cILC3s can currently not be foreseen, given that T cells may be affected by the treatment, too. Finally, the developmental connection between cILC1 subsets, characterized by different levels of CD5 and CD161, is supported by trajectory analysis but needs to be further substantiated, for example, by employing clonal *in vitro* differentiation assays.

RESOURCE AVAILABILITY

Lead contact

Requests for further information and resources should be directed to and will be fulfilled by the lead contact, Sabrina B. Bennstein (sabrina.bennstein1@rwth-aachen.de).

Materials availability

Not applicable.

Data and code availability

scRNA-seq data have been deposited at the database: European Genome-Phenome Archive (EGA) with the accession number: EGAS50000001204 and are publicly available upon reasonable request as of the date of publication. This paper does not report original code. Any additional information required to reanalyze the data reported in this paper is available from the lead contact upon request.

ACKNOWLEDGMENTS

The authors thank the parents for giving their consent to obtain umbilical CB and pediatric blood samples. The authors further thank Dr. Jonas Schulte-Schrepping for providing the R code for the Seurat analyses. This work was funded by the Deutsche Forschungsgemeinschaft (DFG, German Research Foundation), with projects 514891263 and 470195722 (to M.U.). It was further supported by the Elternverein für krebskranke Kinder Krefeld and Helios Forschungsförderung (to T.X.U.P.) and the Forschungskommission (Research Commission) of the Medical Faculty of the Heinrich-Heine-Universität Düsseldorf (to S.B.B.). This project received funding from the Klaus Tschira Boost Fund, a joint initiative of the German Scholars Organization and the Klaus Tschira Foundation (GSO/KT-49 to S.B.B.). This work was supported by the Ministry of Culture and Science of North Rhine-Westphalia. NGS analyses were carried out at the Joint Scientific Facility WGGC-Bonn PRECISE.

AUTHOR CONTRIBUTIONS

Project administration, S.B.B.; conceptualization, S.B.B., M.D.B., and M.U.; investigation, S.B.B., T.X.U.P., and M.D.B.; visualization, S.B.B., J.R., and M.U.; funding acquisition, S.B.B. and M.U.; methodology, S.B.B., J.R., K.R., S.P., E.D.D., and M.D.B.; writing – original draft, S.B.B., J.R., and M.U.; writing – review & editing, S.B.B., J.R., S.P., E.D.D., T.N., M.D.B., and M.U.; resources, J.C.F., G.K., and T.N.; supervision, M.U.

DECLARATION OF INTERESTS

The authors declare no competing interests.

STAR★METHODS

Detailed methods are provided in the online version of this paper and include the following:

- KEY RESOURCES TABLE
- EXPERIMENTAL MODEL AND STUDY PARTICIPANT DETAILS
- METHOD DETAILS
  - Isolation of MNCs from cord blood
  - Flow cytometric analyses
  - Cell sorting
  - Functional analyses
  - Artificial thymic organoid (ATO) model
  - Single-cell RNA sequencing (scRNA-seq) using BD rhapsody
  - scRNA-seq analyses
- QUANTIFICATION AND STATISTICAL ANALYSES

SUPPLEMENTAL INFORMATION

Supplemental information can be found online at https://doi.org/10.1016/j.celrep.2026.117000.

Received: October 7, 2025
Revised: January 9, 2026
Accepted: January 21, 2026
Published: February 17, 2026

REFERENCES

1. Vivier, E., Artis, D., Colonna, M., Diefenbach, A., Di Santo, J.P., Eberl, G., Koyasu, S., Locksley, R.M., McKenzie, A.N.J., Mebius, R.E., et al. (2018). Spits, H: Innate Lymphoid Cells: 10 Years On. Cell *174*, 1054–1066.
2. Bennstein, S.B., and Uhrberg, M. (2022). Uhrberg, M: Biology and therapeutic potential of human innate lymphoid cells. FEBS J. *289*, 3967–3981.
3. Bennstein, S.B., and Uhrberg, M. (2024). Uhrberg, M: Circulating innate lymphoid cells (cILCs): Unconventional lymphocytes with hidden talents. J. Allergy Clin. Immunol. *154*, 523–536.
4. Mazzurana, L., Czarnewski, P., Jonsson, V., Wigge, L., Ringnér, M., Williams, T.C., Ravindran, A., Björklund, Å.K., Säfholm, J., Nilsson, G., et al. (2021). Mjösberg, J: Tissue-specific transcriptional imprinting and heterogeneity in human innate lymphoid cells revealed by full-length single-cell RNA-sequencing. Cell Res. *31*, 554–568.
5. Bennstein, S.B.,, Weinhold, S., Manser, A.R., Scherenschlich, N., Noll, A., Raba, K., Kögler, G., Walter, L., and Uhrberg, M. (2020). Uhrberg, M: Umbilical cord blood-derived ILC1-like cells constitute a novel precursor for mature KIR+NKG2A- NK cells. eLife *9*, e55232.
6. Lim, A.I. (2017). Di Santo, JP: Systemic Human ILC Precursors Provide a Substrate for Tissue ILC Differentiation. Cell *168*, 1086–1100.e10.
7. Bennstein, S.B.,, Scherenschlich, N., Weinhold, S., Manser, A.R., Noll, A., Raba, K., Kögler, G., Walter, L., and Uhrberg, M. (2021). Uhrberg, M: Transcriptional and functional characterization of neonatal circulating ILCs. Stem Cells Transl. Med. *10*, 867–882.
8. Mjösberg, J.M., Trifari, S., Crellin, N.K., Peters, C.P., van Drunen, C.M., Piet, B., Fokkens, W.J., Cupedo, T., and Spits, H. (2011). Human IL-25- and IL-33-responsive type 2 innate lymphoid cells are defined by expression of CRTH2 and CD161. Nat. Immunol. *12*, 1055–1062.
9. Li, S.,, Morita, H., Sokolowska, M., Tan, G., Boonpiyathad, T., Opitz, L., Orimo, K., Archer, S.K., Jansen, K., Tang, M.L.K., et al. (2019). Akdis, CA: Gene expression signatures of circulating human type 1, 2 and 3 innate lymphoid cells. J. Allergy Clin. Immunol. *143*, 2321–2325.
10. Vely, F.,, Barlogis, V., Vallentin, B., Neven, B., Piperoglou, C., Ebbo, M., Perchet, T., Petit, M., Yessaad, N., and Touzot, F. (2016). Evidence of innate lymphoid cell redundancy in humans. Nat. Immunol. *17*, 1291–1299.
11. Jaeger, N., and Colonna, M. (2024). Diversity of group 1 innate lymphoid cells in human tissues. Nat. Immunol. *25*, 1460–1473.
12. Roan, F., Stoklasek, T.A., Whalen, E., Molitor, J.A., Bluestone, J.A., Buckner, J.H., and Ziegler, S.F. (2016). Ziegler, SF: CD4+ group 1 innate lymphoid cells form a functionally distinct ILC subset that is increased in systemic sclerosis. J. Immunol. *196*, 2051–2062.
13. Roan, F., and Ziegler, S.F. (2017). Ziegler, SF: Human Group 1 Innate Lymphocytes Are Negative for Surface CD3; but Express CD5. Immunity *46*, 758–759.
14. Reiß, J.,, Ghosh, S., Scheid, M., Graafen, L., Scherenschlich, N., Weinhold, S., Raba, K., Paulusch, S., De Dominico, E., Pham, T.X.U., et al. (2025). A human NK cell progenitor that originates in the thymus and generates KIR+NKG2A-NK cells. Sci. Adv. *11*, eadv9650.
15. Hochdörfer, T.,, Mjösberg, J., Pardali, K., and Mjösberg, J. (2019). Expression of c-Kit discriminates between two functionally distinct subsets of human type 2 innate lymphoid cells. Eur. J. Immunol. *49*, 884–893.
16. Li, Z.,, and Yu, J. (2024). Therapeutic application of human type 2 innate lymphoid cells via induction of granzyme B-mediated tumor cell death. Cell *187*, 624–641.e623.
17. Campana, S.,, De Pasquale, C., Barberi, C., Oliveri, D., Sidoti Migliore, G., Galletti, B., Guarneri, C., Cannavò, S.P., and Ferlazzo, G. (2021). Ferlazzo, G: Circulating ILC precursors expressing CD62L exhibit a type 2 signature distinctly decreased in psoriatic patients. Eur. J. Immunol. *51*, 1792–1798.
18. Nagasawa, M.,, Heesters, B.A., Kradolfer, C.M.A., Krabbendam, L., Martinez-Gonzalez, I., de Bruijn, M.J.W., Golebski, K., Hendriks, R.W., Stadhouders, R., Spits, H., and Bal, S.M. (2019). KLRG1 and NKp46 discriminate subpopulations of human CD117+CRTH2- ILCs biased toward ILC2 or ILC3. J. Exp. Med. *216*, 1762–1776.
19. Uyen Pham, T.X., Bennstein, S.B., Klumb, J., Niehues, T., and Uhrberg, M. (2022). Circulating Innate Lymphoid Cells (ILCs) in Healthy Children: Reference Values for Evaluation of Treatment in Immunocompromised Pediatric Patients. J. Clin. Immunol. *42*, 1405–1408.
20. Kløverpris, H.N., Kazer, S.W., Mjösberg, J., Mabuka, J.M., Wellmann, A., Ndhlovu, Z., Yadon, M.C., Nhamoyebonde, S., Muenchhoff, M., Simoni, Y., and Leslie, A. (2016). Innate Lymphoid Cells Are Depleted Irreversibly during Acute HIV-1 Infection in the Absence of Viral Suppression. Immunity *44*, 391–405.
21. Teunissen, M.B.M., Munneke, J.M., Bernink, J.H., Spuls, P.I., Res, P.C.M., Te Velde, A., Cheuk, S., Brouwer, M.W.D., Menting, S.P., Eidsmo, L., et al. (2014). Composition of Innate Lymphoid Cell Subsets in the Human Skin: Enrichment of NCR+ ILC3 in Lesional Skin and Blood of Psoriasis Patients. J. Invest. Dermatol. *134*, 2351–2360.
22. Beller, R., Bennstein, S.B., Reinhardt, D., Gauß, G., Chamorra Vina, C., Hanenberg, H., Uhrberg, M., and Götte, M. (2025). Götte, M: Effects of a Low Versus Moderate–High Intense Exercise Program on Innate Immune Recovery, Fitness, and Quality of Life During Pediatric Allo-HSCT—The ANIMAL Exploratory Randomized Controlled Trial. Pediatr. Blood Cancer *72*, e31826.
23. Deppe, I., Beller, R., Kiehl, F., Lazzari, N.D., Bennstein, S.B., Reinhardt, D., Dirksen, U., and Götte, M. (2025). Götte, M: The impact of a single HIIT intervention on the mobilization of NK cells and ILCs in adolescents and young adults (AYA) undergoing cancer treatment: an interventional controlled trial. BMC Cancer *25*, 689.
24. Amling, L., Rink, L., Bennstein, S.B., and Bennstein, S.B. (2025). Short-term oral zinc supplementation enhances Natural Killer cell functionality and decreases circulating Innate Lymphoid Cell counts and frequencies in healthy young adults. J. Transl. Med. *23*, 333.
25. Nagasawa, M., Germar, K., Blom, B., and Spits, H. (2017). Human CD5+ Innate Lymphoid Cells Are Functionally Immature and Their Development from CD34+ Progenitor Cells Is Regulated by Id2. Front. Immunol. *8*, 1047.
26. Xu, W.,, Cherrier, D.E., Chea, S., Vosshenrich, C., Serafini, N., Petit, M., Liu, P., Golub, R., and Di Santo, J.P. (2019). An Id2(RFP)-Reporter

Mouse Redefines Innate Lymphoid Cell Precursor Potentials. Immunity *50*, 1054–1068.e1053.

27. Freud, A.G., Mundy-Bosse, B.L., Yu, J., and Caligiuri, M.A. (2017). Caligiuri, MA: The Broad Spectrum of Human Natural Killer Cell Diversity. Immunity *47*, 820–833.
28. Manser, A.R., Weinhold, S., and Uhrberg, M. (2015). Uhrberg, M: Human KIR repertoires: shaped by genetic diversity and evolution. Immunol. Rev. *267*, 178–196.
29. Caligiuri, M.A. (2008). Human natural killer cells. Blood *112*, 461–469.
30. Manser, A.R., Uhrberg, M., and Uhrberg, M. (2016). Age-related changes in natural killer cell repertoires: impact on NK cell function and immune surveillance. Cancer Immunol. Immunother. *65*, 417–426.
31. Flommersfeld, S.,, Böttcher, J.P., Ersching, J., Flossdorf, M., Meiser, P., Pachmayr, L.O., Leube, J., Hensel, I., Jarosch, S., Zhang, Q., et al. (2021). Fate mapping of single NK cells identifies a type 1 innate lymphoid-like lineage that bridges innate and adaptive recognition of viral infection. Immunity *54*, 2288–2304.e87.
32. Rebuffet, L.,, Melsen, J.E., Escalière, B., Basurto-Lozada, D., Bhandoola, A., Björkström, N.K., Bryceson, Y.T., Castriconi, R., Cichocki, F., Colonna, M., et al. (2024). Vivier, E: High-dimensional single-cell analysis of human natural killer cell heterogeneity. Nat. Immunol. *25*, 1474–1488.
33. Bianca Bennstein, S., Riccarda Manser, A., Weinhold, S., Scherenschlich, N., and Uhrberg, M. (2019). OMIP-055: Characterization of Human Innate Lymphoid Cells from Neonatal and Peripheral Blood. Cytometry A *95*, 427–430.
34. Lam, V.C., Folkersen, L., Aguilar, O.A., and Lanier, L.L. (2019). Lanier, LL: KLF12 Regulates Mouse NK Cell Proliferation. J. Immunol. *203*, 981–989.
35. Seet, C.S., He, C., Bethune, M.T., Li, S., Chick, B., Gschweng, E.H., Zhu, Y., Kim, K., Kohn, D.B., Baltimore, D., et al. (2017). Montel-Hagen, A: Generation of mature T cells from human hematopoietic stem and progenitor cells in artificial thymic organoids. Nat. Methods *14*, 521–530.
36. Tufa, D.M.,, Yingst, A.M., Trahan, G.D., Shank, T., Jones, D., Shim, S., Lake, J., Winkler, K., Cobb, L., Woods, R., et al. (2020). Verneris, MR: Human innate lymphoid cell precursors express CD48 that modulates ILC differentiation through 2B4 signaling. Sci. Immunol. *5*, eaay4218.
37. Kokkinou, E.,, Mjösberg, J., Mazzurana, L., Gutierrez-Perez, I., Tibbitt, C.A., Weigel, W., Soini, T., Carrasco, A., Rao, A., Nagasawa, M., et al. (2022). CD45RA+CD62L- ILCs in human tissues represent a quiescent local reservoir for the generation of differentiated ILCs. Sci. Immunol. *7*, eabj8301.
38. Schilham, M.W., Moerer, P., Cumano, A., and Clevers, H.C. (1997). Clevers, HC: Sox-4 facilitates thymocyte differentiation. Eur. J. Immunol. *27*, 1292–1295.
39. Cook, M.E.,, Bradstreet, T.R., Webber, A.M., Kim, J., Santeford, A., Harris, K.M., Murphy, M.K., Tran, J., Abdalla, N.M., Schwarzkopf, E.A., et al. (2022). Edelson, BT: The ZFP36 family of RNA binding proteins regulates homeostatic and autoreactive T cell responses. Sci. Immunol. *7*, eabo0981.
40. Schmitt, T.M., and Zúñiga-Pflücker, J.C. (2002). Zúñiga-Pflücker, JC: Induction of T Cell Development from Hematopoietic Progenitor Cells by Delta-like-1 In Vitro. Immunity *17*, 749–756.
41. Zúñiga-Pflücker, J.C. (2004). T-cell development made simple. Nat. Rev. Immunol. *4*, 67.
42. Wahlen, S.,, Matthijssens, F., Van Loocke, W., Taveirne, S., Kiekens, L., Persyn, E., Van Ammel, E., De Vos, Z., De Munter, S., Matthys, P., et al. (2022). Leclercq, G: The transcription factor RUNX2 drives the generation of human NK cells and promotes tissue residency. eLife *11*, e80320.
43. Prager, I.,, and Watzl, C. (2019). Watzl, C: Mechanisms of natural killer cell-mediated cellular cytotoxicity. J. Leukoc. Biol. *105*, 1319–1329.
44. Kokkinou, E.,, Soini, T., Pandey, R.V., van Acker, A., Theorell, J., Czarnewski, P., Kvedaraite, E., Vandamme, N., Lourda, M., Sorini, C., et al. (2023). Mjösberg, J: The single-cell transcriptional landscape of innate and adaptive lymphocytes in pediatric-onset colitis. Cell Rep. Med. *4*, 101038.
45. Acuto, O.,, and Michel, F. (2003). Michel, F: CD28-mediated co-stimulation: a quantitative support for TCR signalling. Nat. Rev. Immunol. *3*, 939–951.
46. Haack, S.,, Baiker, S., Schlegel, J., Sauer, M., Sparwasser, T., Langenhorst, D., and Beyersdorf, N. (2021). Beyersdorf, N: Superagonistic CD28 stimulation induces IFN-γ release from mouse T helper 1 cells in vitro and in vivo. Eur. J. Immunol. *51*, 738–741.
47. Lee, J.S.,, Cella, M., McDonald, K.G., Garlanda, C., Kennedy, G.D., Nukaya, M., Mantovani, A., Kopan, R., Bradfield, C.A., Newberry, R.D., and Colonna, M. (2011). Colonna, M: AHR drives the development of gut ILC22 cells and postnatal lymphoid tissues via pathways dependent on and independent of Notch. Nat. Immunol. *13*, 144–151.
48. Chi, X., Jin, W., Zhao, X., Xie, T., Shao, J., Bai, X., Jiang, Y., Wang, X., and Dong, C. (2022). Dong, C: RORgt expression in mature TH17 cells safeguards their lineage specification by inhibiting conversion to TH2 cells. Sci. Adv. *8*, eabn7774.
49. Di Luccia, B., and Huang, S.C.-C. (2019). ILC3s integrate glycolysis and mitochondrial production of reactive oxygen species to fulfill activation demands. J. Exp. Med. *216*, 2231–2241.
50. Linsley, P.S., and Ledbetter, J.A. (1993). The Role of the CD28 Receptor During T Cell Responses to Antigen. Annu. Rev. Immunol. *11*, 191–212.
51. Weng, N-p, Akbar, A.N., Goronzy, J., and Goronzy, J. (2009). CD28+ T cells: their role in the age-associated decline of immune function. Trends Immunol. *30*, 306–312.
52. Maki, G., Klingemann, H.G., Martinson, J.A., and Tam, Y.K. (2001). Tam, YK: Factors regulating the cytotoxic activity of the human natural killer cell line, NK-92. J. Hematother. Stem Cell Res. *10*, 369–383.
53. Zhang, X., Ma, Y., He, Y., Gu, W., Yan, Y., Ji, W., Huang, L., Wang, Y., Hao, C., Li, G., et al. (2022). Foxp2 inhibits Th9 cell differentiation and attenuates allergic airway inflammation in a mouse model of ovalbumin-induced asthma. Int. Immunopharmacol. *111*, 109060.
54. Street, K., Risso, D., Fletcher, R.B., Das, D., Ngai, J., Yosef, N., Purdom, E., and Dudoit, S. (2018). Dudoit, S: Slingshot: cell lineage and pseudotime inference for single-cell transcriptomics. BMC Genom. *19*, 477.
55. Wu, T., Hu, E., Xu, S., Chen, M., Guo, P., Dai, Z., Feng, T., Zhou, L., Tang, W., Zhan, L., et al. (2021). clusterProfiler 4.0: A universal enrichment tool for interpreting omics data. Innovation *2*, 100141.
56. R Team (2020). RStudio: Integrated Development for R (RStudio). http://www.rstudio.com/.
57. R Core Team (2022). R: A Language and Environment for Statistical Computing (R Foundation for Statistical Computing).
58. De Domenico, E., Bonaguro, L., Schulte-Schrepping, J., Becker, M., Händler, K., and Schultze, J.L. (2020). Optimized workflow for single-cell transcriptomics on infectious diseases including COVID-19. STAR Protoc. *1*, 100233.
59. Hao, Y.,, Stuart, T., Kowalski, M.H., Choudhary, S., Hoffman, P., Hartman, A., Srivastava, A., Molla, G., Madad, S., Fernandez-Granda, C., et al. (2024). Dictionary learning for integrative, multimodal and scalable single-cell analysis. Nat. Biotechnol. *42*, 293–304.
60. Satija, R.,, Farrell, J.A., Gennert, D., Schier, A.F., and Regev, A. (2015). Regev, A: Spatial reconstruction of single-cell gene expression data. Nat. Biotechnol. *33*, 495–502.
61. Schulte-Schrepping, J., Reusch, N., Paclik, D., Baßler, K., Schlickeiser, S., Zhang, B., Krämer, B., Krammer, T., Brumhard, S., Bonaguro, L., et al. (2020). Severe COVID-19 Is Marked by a Dysregulated Myeloid Cell Compartment. Cell *182*, 1419–1440.e23.

STAR★METHODS

KEY RESOURCES TABLE

REAGENT or RESOURCE	SOURCE	IDENTIFIER
Antibodies		
Anti human CD3-FITC	Biolegend	Cat# 300405; RRID:AB_ 314059
Anti human CD1a-FITC	Biolegend	Cat# 300104; RRID:AB_ 314018
Anti human CD14-FITC	Biolegend	Cat# 325604; RRID:AB_ 830677
Anti human CD19-FITC	Biolegend	Cat# 302206; RRID:AB_ 314236
Anti human TCR$\alpha\beta$-FITC	Biolegend	Cat# 306705; RRID:AB_ 314639
Anti human TCR$\gamma\delta$-FITC	Biolegend	Cat# 331207; RRID:AB_ 1575111
Anti human CD123-FITC	Biolegend	Cat# 306014; RRID:AB_ 2124259
Anti human CD303/BDCA-2-FITC	Biolegend	Cat# 354208; RRID:AB_2561364
Anti human FcεR1 -FITC	Biolegend	Cat# 334608; RRID:AB_ 1227653
Anti human CD235α -FITC	Biolegend	Cat# 349104; RRID:AB_ 10613463
Anti human CD66b -FITC	Biolegend	Cat# 305104; RRID:AB_ 314496
Anti human CD34-FITC	Biolegend	Cat# 343504; RRID:AB_ 1731852
Anti human CD94-PE/Cy7	Biolegend	Cat# 305516; RRID:AB_ 2632753
Anti human CD56-BV650	Biolegend	Cat# 318344; RRID:AB_ 2563838
Anit human CD117-BV421	Biolegend	Cat# 313216; RRID:AB_ 11148721
Anti human CRTH2-PE/Dazzle594	Biolegend	Cat# 350126; RRID:AB_2572053
Anti human CD161-Alexa Flour 700	Biolegend	Cat# 339942; RRID:AB_2565870
Anti human CD127-PE/Cy5	Beckman Coulter	Cat# A64617; RRID: AB_2833010
Anti human CD28-PE	Beckman Coulter	Cat#I-M2071U; RRID:AB_2833011
Anti human CD3-BV605	Biolegend	BioLegend Cat# 300460; RRID:AB_2564380
Anti human TCR$\gamma\delta$ -APC	Biolegend	BioLegend Cat# 331212; RRID:AB_1089214
Anti-human CD3 biotin	Biolegend	Cat# 317320; RRID:AB_ 10916519
Anti-human CD14-biotin	Biolegend	Cat# 367105; RRID:AB_ 2566617
Anti human CD19-biotin	Biolegend	Cat# 302204; RRID:AB_ 314234

(*Continued on next page*)

Continued

REAGENT or RESOURCE	SOURCE	IDENTIFIER
Anti human CD66b-biotin	Biolegend	Cat# 305120; RRID: AB_2566608
BD™ AbSeq Oligo Rat Anti-Human CD294 (CRTH2)	BD	RRID:940098 https://www.bdbiosciences.com
BD™ AbSeq Oligo Mouse Anti-Human CD34	BD	RRID:940021, https://www.bdbiosciences.com
BD™ AbSeq Oligo Mouse Anti-Human CD1a	BD	RRID:940063, https://www.bdbiosciences.com
BD™ AbSeq Oligo Mouse Anti-Human CD117	BD	RRID:940051, https://www.bdbiosciences.com
BD™ AbSeq Oligo Mouse Anti-Human NKp44 (CD336)	BD	RRID:940085, https://www.bdbiosciences.com
BD™ AbSeq Oligo Mouse Anti-Human CD94	BD	RRID:940081, https://www.bdbiosciences.com
Anti human CD2-BV785	Biolegend	Cat# 300234; RRID:AB_2800717
Anti human CD48-PE	Biolegend	Cat# 336708; RRID:AB_2229041
Anti human CD25-PE/Cy7	Biolegend	Cat# 302612; RRID:AB_314282
Anti human KLRG1-APC/Fire750	Biolegend	Cat# 367718; RRID:AB_2687392
Anti human CD127-APC	Biolegend	Cat# 361316; AB_361316
Anti human Granzyme K-PerCP-eFlour710	eBioscience	Cat# 46-8897-41; RRID:AB_2573853
Biological samples		
Healthy umbilical cord blood	José Carreras Stem Cell Bank at the ITZ, University Hospital Düsseldorf	https://www.uniklinik-duesseldorf.de/patienten-besucher/klinikeninstitutezentren/jose-carreras-stammzellbank
Healthy peripheral blood of children	Helios Klinikum Krefeld	https://www.helios-gesundheit.de/standorte-angebote/kliniken/krefeld/leistungen/fachbereiche/kinder-jugendmedizin/
Critical commercial assays		
LEGENDPLEX Human T helper Cytokine Panel	Biolegend	No identifier available
BD Ab-Seq Immune Discovery Panel	BD	625970, https://www.bdbiosciences.com
MojoSort Streptavidin Nanobeads	Biolegend	Cat# 480016
Fixation buffer	Biolegend	Cat# 420801
Intracellular Staining Permeabilization Wash Buffer (10×)	Biolegend	Cat# 421002
Deposited data		
Accession Number: EGAS50000001204	This paper	European Genome-Phenome Archive (EGA), https://ega-archive.org/
Experimental models: Cell lines		
Cell line (M. musculus) OP9-DL1	Provided by Prof. Dr. Zúñiga-Pflücker, University of Toronto	RRID:CVCL_B218
MS5-mDLL1 Stromal Cell Line	Merck/Sigma-Aldrich	No identifier available, SCC166
Software and algorithms		
GraphPad Prism	www.graphpad.com	GraphPad Prism, RRID:SCR_002798
Kaluza Software	Beckman Coulter	No identifier
Slingshot	Street K et al.[54]	https://doi.org/10.1186/s12864-018-4772-0
Clusterprofiler 4.0	Wu et al.[55]	https://doi.org/10.1016/j.xinn.2021.100141

(*Continued on next page*)

Continued		
REAGENT or RESOURCE	SOURCE	IDENTIFIER
R Studio	R Studi Team[56]	http://www.rstudio.com/.
R	R Team[57]	https://www.R-project.org/.
Other		
Anti human CD28 superagonist	Ancell	Not identifier available, similar to Millipore Cat# 217669-100UG, RRID:AB_10678684

EXPERIMENTAL MODEL AND STUDY PARTICIPANT DETAILS

Umbilical cord blood (CB) samples were collected from the José Carreras Stem Cell Bank at the ITZ. The CBs were all term births (week of gestation: 38 + 5, 40 + 8, 38 + 5). The study is in accordance to the Declaration of Helsinki and was accepted by the institutional review board at the University of Düsseldorf (study number 2019–383). CB samples were processed directly. The CBs were donated anonymously, hence no information on the sex can be provided.

The protocol to use peripheral blood of healthy children was accepted by the institutional review board at the University of Düsseldorf (study number 2018-12) and is in accordance to the declaration of Helsinki. No information on the sex can be provided due to anonymous donations.

The MS5-hDLL1 cell line (Merck) was cultured in DMEM (Gibco) with 10% FCS (Merck). The cell line was tested regularly for mycoplasma.

METHOD DETAILS

Isolation of MNCs from cord blood

CB samples were layered undiluted on a density gradient centrifugation (Biocoll, 1.077 g/cm3/Biochrom Merck Millipore). Next, the cells were incubated for 5min at room temperature (RT) in an ice-cold ammonium chloride solution (pH = 7.4, University Clinic Düsseldorf) to lyse the erythrocytes. Mononuclear cells (MNCs) were washed three times afterward, counted, and either directly used for cell sorting or cryopreserved. Peripheral blood samples were processed in the same way, as previously described.[19]

Flow cytometric analyses

As described previously,[19,33] the cells were stained with the following FITC-conjugated antibodies being part of the lineage panel (Lin): anti-CD3 (UCHT1), anti-CD1a (HI149), anti-CD14 (HCD14), anti-CD19 (HIB19) anti-TCR$\alpha\beta$ (IP26), anti-TCR$\gamma\delta$ (B1), anti-CD123 (6H6), anti-CD303/BDCA-2 (201A), anti-FcεR1a (AER-37(CRA-1)), anti-CD235a (HI264), anti-CD66b (G10F5), and anti-CD34 (581), all from BioLegend. The following antibodies were also used within this study: anti-CD94-PE/Cy7 (DX22), anti-CD3 Brilliant violet (BV) 605 (UCHT1), anti-CD56-BV650 (HCD56), anti-TCR$\gamma\delta$-APC (B1), anti-CD117-BV421 (104D2), anti-CRTH2-PE/Dazzle 594 (BM16), and anti-CD161-Alexa Flour 700 (HP-3G10), anti-CD2-BV785 (RPA-2.10), anti-CD48-PE (BJ40), anti-CD25-PE/Cy7 (BC96), anti-KLRG1(MAFA)-APC/Fire750 (SA231A2), anti-CD127-APC (A019D5), all from BioLegend (California, USA), as well as anti-CD127-PE/Cy5 (R34.34) and anti-CD28-PE (CD28.2), all from Beckman Coulter (California, USA) and anti-Granzyme K-APC (G3H69) from eBioscience (Thermo Fisher Scientific). All flow cytometric analyses were performed on a Cytoflex (Beckman Coulter) with previously described settings.[33] Intracellular staining for Granzyme K was performed according to manufacturer's instructions with a Fixation Buffer and Perm/wash Buffer (both Biolegend). Analyses were performed on the Kaluza software 2.1 (Beckman Coulter).

Cell sorting

As described previously,[5,7] monocytes, T cells, B cells, and granulocytes were depleted prior to sorting using MojoSort Streptavidin Nanobeads (Biolegend) using the negative selection protocol. In brief, $\sim$10-20 $\times$ 10^7 MNCs were stained with the following biotinylated antibodies: anti-CD3 (OKT3), anti-CD14 (63D3), anti-CD19 (HIB19), and anti-CD66b (G10F5) for 15min on ice. After washing, cells were incubated with MojoSort Streptavidin Nanobeads for 15min on ice. After washing, the cells were magnetically separated for 5min, harvested, and further stained for faithful ILC and NK cell identification.[33] The following subsets were bulk sorted: cILC1s as $Lin^-CD94^-CD34^-CD127^+CD117^-CRTH2^-$, cILC2s as $Lin^-CD94^-CD34^-CD127^+CD117^{-/+}CRTH2^+$, cILC3s as $Lin^-CD94^-CD34^-CD127^+CD117^+CRTH2^-$, and NK cells as Lin^-CD94^+ cells. Cell sorting was performed on a MoFlo XDP (Beckman Coulter). The cells were then either used for further processing for scRNAs-seq, the ATO differentiation of cILC1s, or *in vitro* stimulation of cILC3s.

Functional analyses

Sorted cILC3s were cultivated for 5 days either in medium alone, with IL-2 (1000 Units/mL), CD28 superagonist (1μg/mL, Ancell, clone: ANC28.1/5D10), or with IL-2 plus CD28 superagonist. The supernatant was taken and analyzed via the Legendplex Human

T Helper Cytokine Panel (Biolegend) according to manufacturer's instructions. The used medium contained the following: 2/3 DMEM with 4.5g/L glucose (Gibco), 1/3 Ham's F12 (Biochrom AG, Berlin, Germany), 10% human AB serum (Biochrom AG, Berlin, Germany), 1% pencillin/streptomycin (stock: 10,000 U/mL penicillin; 10,000 mg/mL streptomycin, Gibco), 25 μmol/L β-mercapthoethanol (Gibco by Thermo Fischer Scientific), 50 μmol/L sodium-selenit (Sigma Aldrich).

Artificial thymic organoid (ATO) model

The ATO model was executed according to the protocol by Seet et al.[35] According to their published protocol, MS5-hDLL1 were harvested by trypsinization and resuspended in RB27 culture medium containing RPMI 1640 (Corning, Manassas, VA), 4% B27 supplement (ThermoFisher Scientific, Grand Island, NY), 30 μM L-ascorbic acid 2-phosphate sesquimagnesium salt hydrate (Sigma-Aldrich, St. Louis, MO) reconstituted in PBS, 1% penicillin–streptomycin (Gibco), 1% L-glutamine (Gibco), 5 ng/mL recombinant human FLT3 ligand (rhFLT3L), and 5 ng/mL recombinant human IL-7 (rhIL-7) (both from Miltenyi). The medium and the 30 μM L-ascorbic acid 2-phosphate sesquimagnesium salt hydrate solution were freshly made once a week. Either freshly sorted $CD34^+$ cells, cILC1s, or NK cells (3×10^2 to 1×10^5 cells) were added to 1×10^5 MS5-hDLL1 cells. The respective cells mixtures were centrifuged 5 min for 300g at 4°C. The supernatant was discarded, and the cell pellet was pipetted carefully on a 0.4μm mesh, which was pre-soaked in RB27 medium. The mesh with the cell pellet was carefully placed in a 6-well plate containing 2mL of RB27. 1mL of medium was changed every 3–4 days. Cell pellets were analyzed after 29 days using flow cytometry with the Kaluza 2.1 software.

Single-cell RNA sequencing (scRNA-seq) using BD rhapsody

The freshly sorted cILC subsets and NK cells were individually multiplexed per donor and per population. In total 12 different oligo-coupled sample tag antibodies (BD Single-Cell Multiplexing Kits, BD) were used to identify each of the four sorted populations of the three donors (3 donors x 4 populations: cILC1s, cILC2s, cILC3s, and NK cells). After the multiplexing step, equal amounts of cells per sample tag were pooled. The pooled samples were stained with the BD Ab-Seq Immune Discovery Panel (Table S1) plus six additional Ab-Seq antibodies (anti-CD34 (clone: 581), anti-CD117 (clone: YB5.B8), anti-CD1a (clone: HI149), anti-CD94 (clone: HP-3D9), CD336 (NKp44, clone: p44-8), and CD294 (CRTH2, clone: BM16), all from BD). The Rhapsody device was loaded with a total of 60.000 multiplexed and Ab-Seq-stained cells. The following single-cell capture and cDNA synthesis as well as exonuclease treatment was performed according to the manufacturer's instructions and published protocol.[58] After these steps, the cDNA sample was stored at 4°C. Library preparation and sequencing was performed at PRECISE, DZNE, Bonn. The libraries were prepared following the manufacturer's instructions and the final products were quantified using a Qubit Fluorometer with the Qubit dsDNA HS Kit (ThermoFisher) and the size-distribution was measured using the Agilent high sensitivity D5000 assay on a TapeStation 4200 system (Agilent technologies). Sequencing was performed in paired-end mode (R1 85bp and R2 215) on a NovaSeq_6000 system with a NovaSeq S4, 300bp. v1.5 chemistry.

The raw Illumina BCL files were demultiplexed with bcl2fastq2 (v2.20), generating paired-end FASTQ files for each library. These FASTQs were then processed with the BD Rhapsody Sequence Analysis Pipeline (v2.2.1), aligning reads to the Gencode GRCh38 human reference genome. For cell identification, we deviated from the default transcript-based calling and employed AbSeq-derived protein-tag reads (AbSeq mode) to define cellular barcodes (https://bd-rhapsody-bioinfo-docs.genomics.bd.com/top_introduction.html).

scRNA-seq analyses

Seurat (Version_4.3.0) was used for scRNA-seq analyses[59,60] with R (Version 4.2.1)[57] and R studio (Versions 2022.07.2).[56] After quality analyses with Seurat, a total of 14032 cells passed initial quality control for pre-filtering, and 13808 cells remained post-filtering with a mitochondrial percentage (percent.mito) cut-off at 25, nFeature_RNA between 200 and 10000, and n_count_RNA >500. RunPCA was used with VariableFeatures, ElbowPlot, and JackStrawPlot to determine 13 dimensions (dims) for RunUMAP in analyses for Figure 1. Clustering was performed with FindNeighbors (13 dims) with a resolution of 0.5 for the scRNA-seq data of all three cILC subsets as well as NK cells (Figure 1), and 9 dims with a resolution of 0.7 for individual cILC1 analyses (Figure 2), and a resolution of 0.4 for individual cILC2 (Figure 3) and cILC3 (Figure 4) analyses. Sub-clustering of cILC1 (Figure 2), cILC2 (Figure 3), and cILC3 (Figure 4) were performed according to the sorted original cell population based on the used sample tags. Cluster markers were calculated with FindAllMarkers and the top 10 differentially expressed genes are displayed. Gene ontology pathways were calculated using the R package ClusterProfiler.[55] Cell lineages were analyzed with the R package Slingshot.[54] The R code used for the scRNA-seq analyses was generously provided by Dr. Jonas Schulte-Schrepping[61] and modified for the purpose of this study. The code for Ab-seq data was taken from https://satijalab.org/seurat/archive/v3.2/multimodal_vignette.html.

For validation of the CB ILCs, we have used the published scRNA-seq data from Jaeger et al. 2024[11] and Reiβ et al. 2025.[14] We have downloaded the Seurat files from their Figure 1A (Blood) and Figure 2D (Tonsil) (Jaeger et al.). We have extracted the top 25 enriched genes from their original analyses from Cluster 0 for ILC2 genes, Cluster 1 for ILCP genes, and Cluster 5 for CILC-like genes from the peripheral blood data and Cluster 8 for ILC3 genes from the tonsil data. Furthermore, we used our previously published data from thymic ILC1s.[14] We have used the command AddModuleScore to highlight the top 25 of these corresponding genes in our datasets.

QUANTIFICATION AND STATISTICAL ANALYSES

Statistical tests were performed with a parametric or nonparametric assumption (depending on normal distribution) and a 0.05 significance level. All analyses were done using GraphPad Prism 10.4.1 (GraphPad Software, San Diego, California USA, www.graphpad.com). Statistical details can be found within the legend of Figure 4 and within the Supplementary Figure legends. In Figure 4E, Wilcoxon t-tests were used to determine differences in $CD28^+$ and $CD28^-$ cILC3 frequencies, their CD117 as well as CD161 MFI. These bar graphs contain data of n = 8–9, where each n represents an individual donor. IFNγ secretion was calculated with a non-parametric ANOVA (Kruskal-Wallis Test) with Dunn′s multiple comparison test with n = 4–9, each n representing an individual donor. The height of the bars represents the mean ± SEM. Each n represents an individual donor in this study.